

# Author's Accepted Manuscript

Rechargeable batteries based on anion intercalation  
graphite cathodes

Miao Zhang, Xiaohe Song, Xuewu Ou, Yongbing  
Tang



PII: S2405-8297(18)30379-9  
DOI: <https://doi.org/10.1016/j.ensm.2018.04.023>  
Reference: ENSM375

To appear in: *Energy Storage Materials*

Received date: 31 March 2018  
Revised date: 18 April 2018  
Accepted date: 21 April 2018

Cite this article as: Miao Zhang, Xiaohe Song, Xuewu Ou and Yongbing Tang, Rechargeable batteries based on anion intercalation graphite cathodes, *Energy Storage Materials*, <https://doi.org/10.1016/j.ensm.2018.04.023>

This is a PDF file of an unedited manuscript that has been accepted for publication. As a service to our customers we are providing this early version of the manuscript. The manuscript will undergo copyediting, typesetting, and review of the resulting galley proof before it is published in its final citable form. Please note that during the production process errors may be discovered which could affect the content, and all legal disclaimers that apply to the journal pertain.

# Rechargeable batteries based on anion intercalation graphite cathodes

## Rechargeable batteries based on anion intercalation graphite cathodes

Miao Zhang, Xiaohe Song, Xuewu Ou, Yongbing Tang\*

Functional Thin Films Research Centre, Shenzhen Institutes of Advanced Technology, Chinese Academy of Sciences, Shenzhen, 518055, China.

Email: tangyb@siat.ac.cn

### Abstract

Owing to the low cost, abundance and high working voltage, graphite cathodes have attracted tremendous attention in rechargeable batteries, especially in aluminum ion batteries (AIBs) and dual-ion batteries (DIBs). In this review, firstly, a general introduction is given to distinguish the working mechanism of graphite from the conventional metal oxide used as cathode in batteries. Secondly, the characterization methods of anion intercalated compounds, theoretical simulation of anion intercalation behavior into the graphitic cathode and the kinetic study of anion diffusion in graphite are discussed. Then, progresses and challenges of AIBs with different types of graphite cathode materials are presented. Next, typical DIBs systems with graphite cathode, a variety of anodes and electrolytes are introduced in detail. Finally, a conclusion for battery systems with anion

intercalation graphite cathodes is draw, and a perspective is outlined to address the existing technical barriers that need to be overcome in future research direction.

## Keywords

Anion intercalation, Aluminum ion batteries; Dual ion batteries; Graphite cathodes

## Contents

Abstract.....	1
Keywords.....	1
Contents.....	2
1. Introduction .....	2
1.1 Background.....	2
1.2 Working mechanisms of different rechargeable batteries .....	4
2. Structure of graphitic cathode and characterization of anion intercalation compounds .....	7
2.1 Structure of graphitic cathode.....	7
2.2 Characterization of anion intercalation graphitic compounds .....	8
2.2.1 XRD.....	9
2.2.2 Raman spectroscopy .....	10
2.3 Theoretical investigation of anion intercalation behavior in the graphitic cathode .....	12
2.4 Kinetic study of anion intercalation in graphite cathode .....	14
2.5 Factors on the electrochemical performance of the batteries with anion intercalation graphite cathode .....	15
2.5.1 Solvent and operation voltage window.....	15
2.5.2 Salt type or anion size.....	17
3. The application of anion intercalation cathode in aluminum ion batteries .....	18
3.1 The rise of AIBs with anion intercalation cathode.....	18
3.2 The booming of AIBs with anion intercalation cathode .....	21
3.3 The challenges of AIBs with anion intercalation cathode.....	27
4. The application of anion intercalation cathode in dual-ion batteries .....	28
4.1 DIBs based on lithium ion electrolyte .....	28
4.1.1 Graphite cathode-metal oxide anode DIBs.....	28
4.1.2 Graphite cathode-graphite/reduced graphene-based anode DIBs .....	29
4.1.3 Graphite cathode- metal anode DIBs.....	32
4.2 Other metal ion based DIBs.....	38
4.3 Hybrid anion DIBs.....	38
5. Conclusion and perspective .....	43
Acknowledgements .....	46

## 1. Introduction

### 1.1 Background

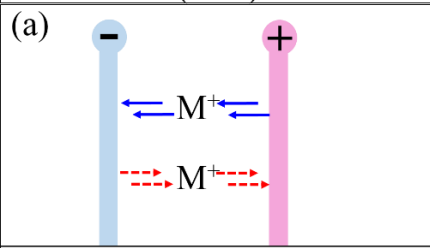
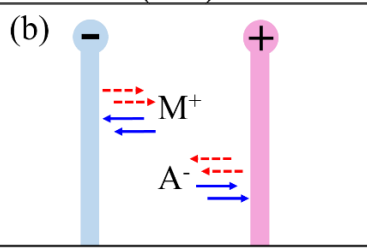
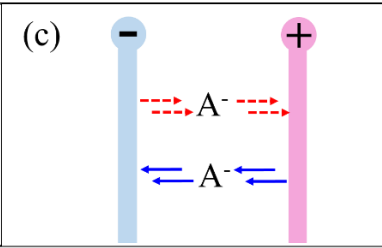

A rechargeable battery is an electrochemical device that can store electrical energy as chemical energy in its anode and cathode during the charging process, and releases the energy as electrical output during the discharging process [1-3]. An ideal rechargeable battery is expected to have high energy density, high power density, long cycle life, excellent environmental compatibility and low cost [4-15]. Metal ion batteries (MIBs), including lithium ion batteries (LIBs), sodium ion batteries (SIBs) and potassium ion batteries (PIBs) *et al.* are typical rechargeable batteries, which rely on the metal ions shuttling between the anode and cathode to realize charging and discharging. Among them, LIBs, which possess the merits of long cycle life, high energy and power density and no memory effect, have dominated the battery market of portable electronics and electric vehicles for around two decades and are as well widely used in grid-scale energy storage [5, 16-20]. Despite currently enormous successes in portable electronics and electric vehicles (EVs), LIBs are limited in meeting the growing demand for higher energy and power densities [21-40]. In another aspect, LIBs are plagued by the shortage and high cost of resource metals (Li, Co, Ni *etc.*) needed in the battery manufacture, and the corresponding environmental pollution of abandoned batteries [17, 41, 42]. Therefore, searching for novel electrode materials, especially cathode materials that of resource-abundant and easily recyclable properties, is in great demand [1].

Graphite is a unique layered structure composed of graphene layers stacked together by the van

der Waals force. Since its interlayer space are highly tunable, graphite can accommodate a variety of ions and molecules to form graphite intercalation compounds (GICs), which display applications in electrical, electrochemical and chemical industries because of their unique physicochemical properties. For instance, the reversible intercalation/de-intercalation of metal ions ( $\text{Li}^+$ ,  $\text{Na}^+$  and  $\text{K}^+$  *et al.*) into/from the graphite makes it widely used as anodes for MIBs. Although comparatively less developed, graphite, which have also exhibited the reversible intercalation and de-intercalation of anions such as hexafluorophosphate anion ( $\text{PF}_6^-$ ), bis(trifluoromethanesulfonyl)imide anion (TFSI) [43-48], is becoming a promising cathode materials in dual-ion batteries (DIBs), hybrid electrochemical capacitors (ECs) [49, 50] and aluminum ion batteries (AIBs). Among these, DIBs and AIBs are gaining more attention since they have obvious advantages over conventional MIBs: 1) lower cost and resource abundance compared to conventional metal oxide cathode in MIBs; 2) higher voltage, which benefits for a higher energy density [51, 52].

## 1.2 Working mechanisms of different rechargeable batteries

As a typical example of MIBs, LIB usually consists of anode generally made of graphite materials, Si-based materials [53, 54] and recently developed lithium metal anodes [55-66]), cathode using lithium-containing transition metal oxide [19, 67-70], such as  $\text{LiCoO}_2$ ,  $\text{LiMn}_2\text{O}_4$ ,  $\text{LiFePO}_4$  *etc.*, and an electrolyte filled separator that allows Li ion transfer but prevents electrodes from direct contact [71, 72]. The charge/discharge mechanism of LIBs is based on the rocking-chair concept, which means repeatedly insertion/extraction of Li ions into/from the anode and the cathode during the charge and discharge process (**Figure 1a**) [4, 16, 18, 19, 21, 42, 67-70, 73, 74].

Metal ion batteries (MIB)	Dual ion batteries (DIB)	Aluminum ion batteries (AIB)*
(a) 	(b) 	(c) 
		
Typical systems		
<p>⊕ <b>LiCoO<sub>2</sub></b> (lithium reaction)</p> <p>⊖ <b>Graphite</b> (lithium reaction)</p>	<p>⊕ <b>Graphite</b> (anion reaction)</p> <p>⊖ <b>Al</b> (lithium reaction)</p>	<p>⊕ <b>Graphite</b> (anion reaction)</p> <p>⊖ <b>Al</b> (electrolyte deposition)</p>
<p>⊕ <math>\text{LiCoO}_2 \leftrightarrow \text{Li}_{1-n}\text{CoO}_2 + n\text{Li} + ne^-</math></p> <p>⊖ <math>6\text{C} + n\text{Li}^+ + ne^- \leftrightarrow \text{C}_6\text{Li}_n</math></p>	<p>⊕ <math>n\text{C} + \text{PF}_6^- \leftrightarrow \text{C}_n[\text{PF}_6] + e^-</math></p> <p>⊖ <math>\text{Al} + \text{Li}^+ + e^- \leftrightarrow \text{AlLi}</math></p>	<p>⊕ <math>\text{C}_n + \text{AlCl}_4^- \leftrightarrow \text{C}_n[\text{AlCl}_4] + e^-</math></p> <p>⊖ <math>4\text{Al}_2\text{Cl}_7^- + 3e^- \leftrightarrow \text{Al} + 7\text{AlCl}_4^-</math></p>

**Figure 1.** Summary of characteristic metrics and typical example systems of metal ion batteries (MIBs) (a), dual ion batteries (DIBs) (b) and aluminum ion batteries (AIBs) (c), where  $M^+$  and  $A^-$  stand for cation and anion, respectively. \*AIB here refers in particular to aluminum ion batteries with graphitic cathode materials and follow the battery working mechanism as shown in **Figure 1c**.

Different from MIB, in DIBs or AIBs, the cathode is replaced by anions intercalation materials. In detail, for DIBs, unlike conventional MIBs, it relies on the intercalation/reaction of both cations and anions into/with the anode and cathode when charged and the extraction/release of these ions back into the electrolyte when discharged. **Figure 1b** clearly illustrates the working mechanism of DIBs using graphite as cathode and Al foil as anode material. During the charging process, the  $\text{Li}^+$  cations alloyed with the Al anodes, and the  $\text{PF}_6^-$  anions intercalated into the graphite cathodes, simultaneously. While for the discharging process, the  $\text{Li}^+$  and  $\text{PF}_6^-$  ions diffuse back into the electrolyte. This charging/discharging process involving both anions and cations is similar to hybrid electrochemical capacitors (ECs) [75-78], but they are still different in working mechanisms

especially at the cathode side [79, 80]. Particularly, the intercalation/de-intercalation of anions at the graphite cathode enables a high cut-off potential up to around 5 V [81, 82], which is favorable for high energy density. In addition, instead of high-cost lithium-containing transition metal oxide cathode, utilizing graphite as cathode can effectively lower the overall cost, and reduce potential environmental pollutions. Furthermore, the versatile replacing of lithium cations into more abundance alkali metal cations is another appealing advantage of DIBs.

AIBs [83-85], developed along with sodium [35, 36, 40, 86-89], potassium [37], calcium [90-93] and magnesium [94-97] based batteries, are considered as candidates for rechargeable batteries which are potentially more cost-effective than lithium. Generally, AIBs can operate in aqueous[98] and non-aqueous (particularly in ionic liquid) electrolyte [99]. The output voltage of aluminum batteries employing aqueous electrolyte is limited by the electrochemical window for water decomposition ( $\sim 1.23\text{V}$ ) [52], while the non-aqueous one using chloroaluminate melts, denoted as  $\text{XCl-AlCl}_3$ , where  $\text{X}^+$  can be a monovalent cation or an organic cation, can operate at a higher voltage. On the other hand, aluminum battery cathode materials such as transitional metal oxide [100], sulfur [84, 101] and oxygen [102, 103], could reversibly react with  $\text{Al}^{3+}$  ions, but devices with these cathode materials are suffering from low operation voltage and short cycle life [52]. As an alternative, carbon-based materials which can accommodate the chloroaluminate anion rather than  $\text{Al}^{3+}$  ions represents a promising candidate as cathode materials for aluminum batteries. For example, Dai's group [104] recently reported a rechargeable aluminum battery with high operation voltage and long cycle life with aluminum metal as anode and three-dimensional graphitic foam as cathode. In their work, the battery operates by the electrochemical deposition and dissolution of aluminum at the anode, and intercalation/de-intercalation of chloroaluminate anions ( $\text{AlCl}_4^-$ ) in the graphite, using a

non-flammable ionic liquid electrolyte (**Figure 1c**). Carbon-based materials cathode hosting the chloroaluminate anion has the same intercalation/de-intercalation reaction mechanism as the cathode in DIBs [105]. In the following discussion of this review, only AIBs with graphite-based materials hosting the  $\text{AlCl}_4^-$  are considered and the case of  $\text{Al}^{3+}$  are beyond the scope.

As far as we know, Ji *et al.* summarized the challenges, the recent progress, and pointed out future directions in the DIBs field [51], however, a comprehensive review about anion intercalation graphite cathode materials, devices and mechanisms are rarely published. In this review, we will present a broad overview of anion intercalation graphite cathode and distinguish the operation difference between anion intercalation devices and conventional MIBs. We will specially outline anion intercalation graphite cathode, including characterization of anion intercalation process, theoretical investigation of anion intercalation behavior and kinetic study of anion diffusion in graphite cathode. Then, a survey of recent work in the area of DIBs and AIBs will follow. Lastly, a conclusion and an overlook on future developments will be presented.

## **2. Structure of graphitic cathode and characterization of anion intercalation compounds**

### **2.1 Structure of graphitic cathode**

Graphite materials generally contain polyaromatic rings with  $\text{sp}^2$  carbon atoms, which are stacked together by  $\pi$ - $\pi$  interaction of the electronic network [106]. The large  $\pi$ -electronic network in graphite can either be easily oxidized or reduced. When an electronegative species accepts an electron and forms an ionic bond with this  $\pi$ -electronic network, an acceptor-type graphite intercalation compounds (GICs) is generated [43]. In contrast, a metal atom can donate an electron to



the network and form a donor-type GIC. Graphite as a cathode material works as an acceptor-type graphite intercalation compounds [47]. GIC is characterized by the stage effect, where the term ‘stages’ refers to the number of graphite layers (denoted as  $m$ ) that lie between alternate intercalant layers. For example, stage 3 means that adjacent intercalant layers are separated by 3 graphene layers. In defining the stages in GIC systems, it is assumed that the graphite material is defect-free and the guest species intercalate as a continuous phase in the graphite lattice. The calculation method of “stage  $m$ ” of a GIC will be presented in the following section. GICs could reversibly intercalate and de-intercalate without any damage to the defect-free graphite lattice, thus it is desirable to adopt GICs for electrochemical applications [43, 44, 107].

## 2.2 Characterization of anion intercalation graphitic compounds

A wide variety of techniques are currently available to study anion intercalated graphite compounds (AIGC). The chemical properties and composition of AIGC are measured by X-ray photoelectron spectra (XPS) and Auger electron spectroscopy (AES). To get the carbon hybrid information of AIGC at different charge and discharge state, X-ray absorption spectroscopy (XAS) is performed to investigate carbon’s bonding environment [44, 45, 108-110], scanning electron microscopy (SEM) has been in use for check the morphology change, and transmission electron microscopy (TEM) is conducted to identify intercalation domains and even line defects [43]. Moreover, electrochemical characterization, such as cyclic voltammetry and impedance spectroscopy, can provide the interfacial kinetics and the impedance characteristics of the battery system [81, 82, 111-116]. Intercalation stages, surface exfoliation during charge/discharge can be evaluated via ex-situ/in-situ and X-ray diffraction (XRD) and Raman, which will later be introduced in detail.

### 2.2.1 XRD

XRD, as one of the most widely used techniques for characterizing the lattice structure of the host, is commonly employed to determine the relationship between the electrochemical behavior and the structural evolution of intercalated graphitic compounds [108]. The pristine graphite electrode exhibits the typical graphite XRD pattern. While upon the anion intercalation, the main XRD peak assigned to pure graphite will be shifted to new positions, which are associated with the anion intercalation caused periodic rearrange of the occupied and unoccupied interlayers between the graphene planes, *i.e.* the stage effect, wherein the intercalated stage number can be calculated through the most intense and the second most intense reflections.

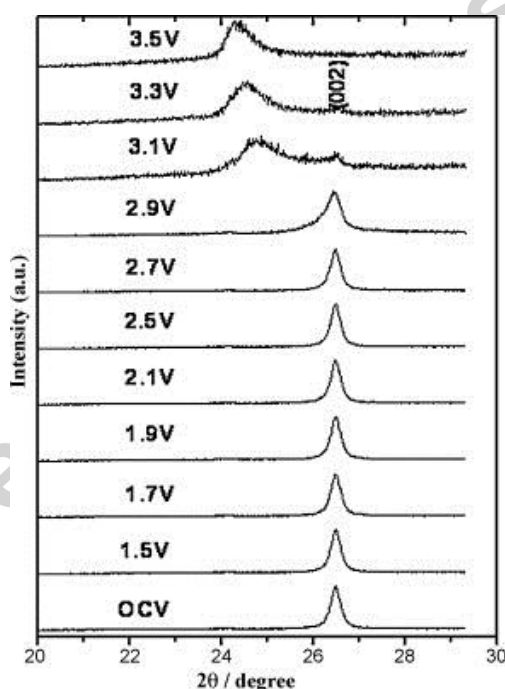


**Figure 2.** In situ XRD patterns of the KS-6 graphite positive electrode in the KS-6/TiO<sub>2</sub> rutile full cell during charging to 3.5 V [109]. Copyright (2010) Elsevier Ltd. All rights reserved.

To better illustrate the stage effect, we exemplified a typical XRD pattern of a graphitic cathode from KS-6 graphite/TiO<sub>2</sub> electrochemical cell, with carbonic acid ester solvent containing PF<sub>6</sub><sup>-</sup> as

electrolyte [109]. In situ XRD experiments were conducted to investigate the reaction mechanisms and structural changes of the KS-6 cathode in the KS-6/TiO<sub>2</sub> full cell with charging up to 3.5V (cutoff voltage of the cell) (**Figure 2**). The (002) peak at 26.5° corresponding to a well-ordered graphite structure with interlayer spacing of 3.35Å. As shown from the in situ XRD pattern, the (002) peak remains at its original position until voltage went up to 2.9V. As the voltage increases to above 3.1 V, the (002) diffraction peak starts to shift to a lower angle. At 3.5 V, the (002) diffraction peak at 26.5° was totally vanished, and a new peak at lower angle of 24.2° appeared. The stage number of  $m$  of the PF<sub>6</sub><sup>-</sup> graphite intercalated is calculated by the equation.

$$m = \frac{d_{00(n+1)}}{d_{00n} - d_{00(n+1)}} \quad (1)$$

Where  $d_{00n}$  and  $d_{00(n+1)}$  denoted the interplanar spacing corresponding to peak (0 0  $n$ ) and (0 0  $n + 1$ ) is according to the Bragg's law. Based on the above equation, calculated stage number of GIC in this work is 3.

### 2.2.2 Raman spectroscopy

Raman scattering during charging/discharging experiments is also widely utilized to investigate the changes of graphite structure during battery operation [117, 118]. Specifically, the G and 2D Raman peaks change in shape, position and relative intensity reflects the evolution of the electronic structure and electron–phonon interactions of anion intercalated graphite.

For example, Dai *et al.* [117] adopted Raman spectroscopy to investigate the changes of the graphite structure during charge/discharge process. As shown in **Figure 3**, **Figure 3(a-d)** illustrate the evolution of the graphite G bond during charge/discharge at a rate of 50 mA g<sup>-1</sup>, suggesting high graphite structural integrity during anion (AlCl<sub>4</sub><sup>-</sup>) intercalation/de-intercalation cycles. At the

beginning of lower plateau charging process, the G band of pristine graphite ( $1,584\text{ cm}^{-1}$ ) shifted by  $\sim 20\text{ cm}^{-1}$ , resulting from rearrangement of positive charges on the boundary layers of the graphite that caused by  $\text{AlCl}_4^-$  intercalation. Boundary layers adjacent to intercalant layers, leading to a large blue shift in the  $E_{2g}$  band for these layers, and consequently giving rise to two different  $E_{2g}$  peaks overall, (inner (i) and outer (b) (**Figure 3a**, Inset; spectra in red)). Based on the ratio of the intensities of inner and outer peaks ( $I_i$  and  $I_b$ ), the intercalation stage ( $m > 2$ ) can be calculated based on equation (2):

$$\frac{I_i}{I_b} = \frac{\sigma_i (m-2)}{\sigma_b} \quad (2)$$

$\sigma_i/\sigma_b$  corresponds to the ratio of Raman scattering's cross-sections, which is assumed to be unity. (The  $E_{2g(b)}$  band then underwent a small splitting ( $\sim 3\text{ cm}^{-1}$ ) at 1.94-1.99 V (**Figure 3a**, Inset spectra in green). At this point, the stage number ( $m$ ) was calculated to be  $\sim 2.5$ . Shortly afterward (at 2.03 V), the  $E_{2g(i)}$  band disappeared completely. This was followed by the  $E_{2g(b)}$  roughly doubling in intensity before it underwent another large splitting ( $1,619\text{--}1,632\text{ cm}^{-1}$ ) at the beginning of the upper plateau ( $\sim 2.097\text{ V}$ ) (**Figure 3a**, spectra in blue). At the fully charged state, only one high-intensity peak at  $1,632\text{ cm}^{-1}$  remained, suggesting the formation of a stage 1 or 2 GIC because neither  $E_{2g(i)}$  and  $E_{2g(b)}$  bands were present. A stage 2 GIC was assumed, based on the capacity of the Al battery. The subsequent discharge process was consistent with the charge process, demonstrating reversibility. (**Figure 3c**).

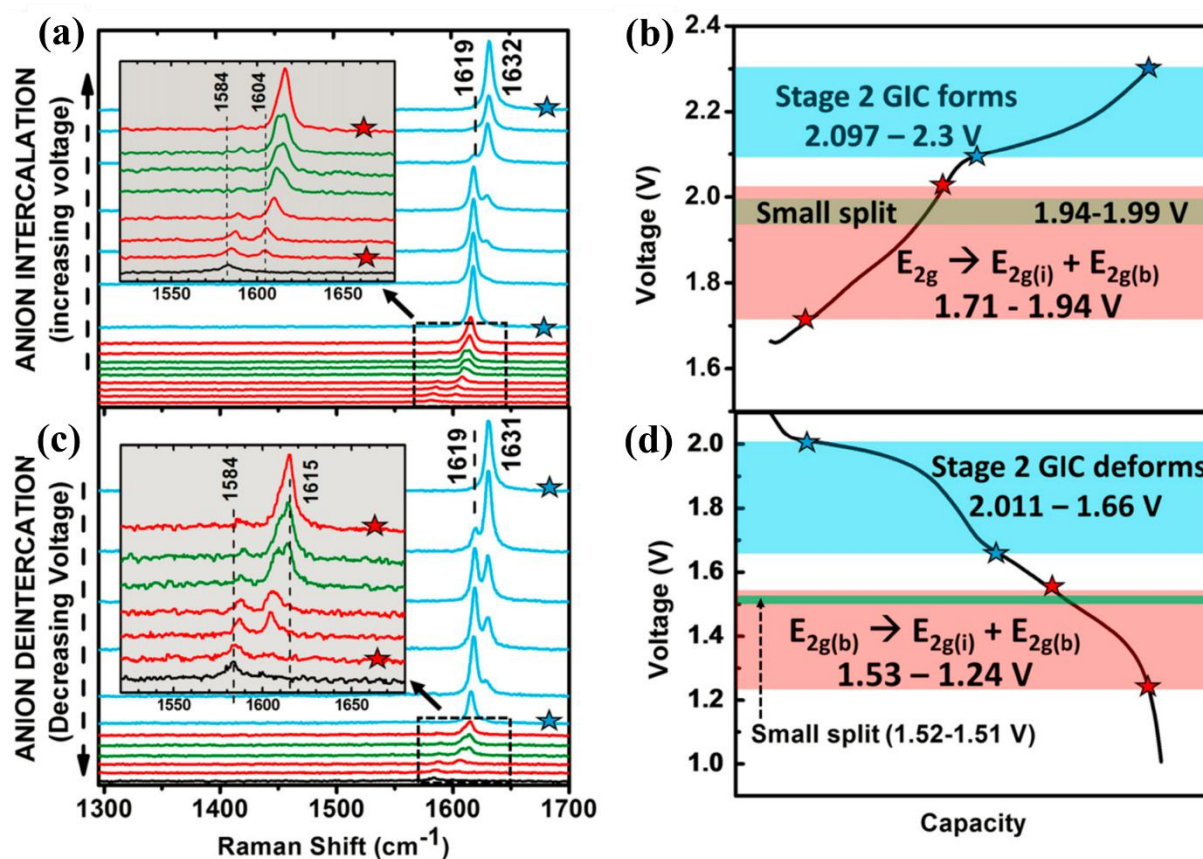


**Figure 3.** In situ Raman spectra of the graphite electrode recorded during (a) charge and (c) discharge at  $50 \text{ mA g}^{-1}$ . (Insets) Zoom-ins on lower voltage spectra corresponding to graphite G band  $E_{2g} \rightarrow E_{2g(i)} + E_{2g(b)}$  splitting (spectra in red, corresponding to red-haded section of charge/discharge curves; spectra in green, corresponding to green-shaded section of charge/discharge curves). The black spectrum in each corresponds to open circuit voltage = 1V, G band =  $1,584 \text{ cm}^{-1}$ . Spectra in blue (corresponding to upper plateau, shaded in blue on charge/discharge curves) represent stage 2GIC formation/deformation. (b) Galvanostatic charging curve ( $50 \text{ mA g}^{-1}$ ), color coordinated with Raman spectra in (a). (d) Galvanostatic discharging curve ( $50 \text{ mA g}^{-1}$ ) color coordinated with Raman spectra in (c) [117].

### 2.3 Theoretical investigation of anion intercalation behavior in the graphitic cathode

Theoretical study, of which two commonly used methods are density functional theory (DFT)

and classical molecular dynamics (MD) simulation, is highly beneficial to gain deeper insight on the materials' working mechanism at atomic level. Because of the unique stage effect, GICs are commonly viewed as periodic structure and can usually be condensed to a unit cell with atom-number less than two hundreds, to which DFT can perform rather effectively and accurately. Therefore, DFT are mostly used to investigate the anion intercalation behavior into graphite, including the thermal stability, electronic structure, Bader charge, voltage and diffusion barrier *etc.* [85, 99, 119-121]. DFT-D2 [122] and DFT-D3 [123] approaches are commonly used for the correction of van der Waals interaction. Ab initio Molecular Dynamic Simulation (AIMD) is to test the thermal stability of the calculation-derived GICs structure. The climbing image-nudged elastic band (CI-NEB) method [124] are used to calculate the diffusion barriers of anions in graphite interlayer.

Tasaki studied graphite respectively intercalated with potassium, lithium, lithium solvated by dimethyl sulfone, lithium solvated by dibutoxy ethane, perchlorate ( $\text{ClO}_4^-$ ), and hexafluorophosphate ( $\text{PF}_6^-$ ) by adopting DFT study, and revealed a strong correlation between the intercalation energy and the electron transfer between the intercalate and graphite[119]. The correlation between the size of the intercalate and the interlayer distance was observed as well. Tasaki concluded that the ionization potential or the electron affinity of the intercalate, along with the size of the intercalate, can be a good measure for the stability of the resulting GIC in general. As AIBs getting more and more attention, DFT study mainly focuses on anion intercalation especially  $\text{AlCl}_4^-$  intercalated graphite [85, 99, 120, 121]. Among these study, one of the most interesting issue is the the structure of  $\text{AlCl}_4^-$ . Debate arise as to whether the  $\text{AlCl}_4^-$  unit it is planar [120] or tetrahedral [121]. The dispute originated from the experimentally observed interlayer space of around

5.286 Å [104], which is smaller than the size of a tetrahedral  $\text{AlCl}_4^-$  unit 5.7 Å. The above mentioned DFT studies take the  $\text{AlCl}_4^-$  intercalated graphite as the only object; Agiorgousis *et al.* [99] later took the electrolyte into consideration and was in good agreement with the experiment. According to the theoretical calculated binding energy and calculated voltage, the tetrahedral  $\text{AlCl}_4^-$  is more likely to be the real configuration. Notably, they as well proposed a novel tetrahedral  $\text{AlCl}_4^-$  configuration between the graphene-layers. Based on the  $\text{AlCl}_4^-$  configuration as Jung *et al.* [121] and Bhauriyal *et al.* [85] use DFT calculation to study the thermal stability, electronic structure, Bader charge, voltage, diffusion barrier to explore staging mechanism.

In another aspect, MD system can effectively tackle system with large amount of atoms at different temperature and electrode potential, and provide useful statistical data, thus it has been widely used to study the electrochemical energy storage system. It's interesting that Eduardo M. Perassi *et al.* [125] employ a theoretical model to determine intercalation entropy and enthalpy of Li-graphite intercalation compound by modeling it as a lattice-gas and performing grand canonical Monte Carlo simulations. They correctly reproduced the main features of the experimental intercalation entropy and enthalpy. As to the anion-related graphite system, the MD study focused on supercapacitor for which electrolyte/graphite interface are of crucial importance. However, as far as we know, there hasn't been any MD study on anion intercalation graphite for battery cathode.

## 2.4 Kinetic study of anion intercalation in graphite cathode

The superior rate property of DIBs and AIBs could possibly be attributed to rapid diffusion of anions in graphitic carbon. Electrochemical techniques, such as the galvanostatic intermittent titration technique (GITT) and electrochemical impedance spectroscopy (EIS), to

determine the chemical diffusion coefficient of anion in graphite. Using cells with 1 M, 3.1 M, and 3.7 M LiPF<sub>6</sub>/DMC, Ishihara *et al.* [126] estimated the chemical diffusion constant of PF<sub>6</sub><sup>-</sup> to be around 10<sup>-12</sup> cm<sup>2</sup> s<sup>-1</sup> by adopting the GITT and EIS. Notably, diffusion coefficients for PF<sub>6</sub><sup>-</sup>, despite the larger molecule size, is higher than that of lithiated oxide in cathode materials such as LiFePO<sub>4</sub>. To further confirm the rapid diffusion of PF<sub>6</sub><sup>-</sup>, a DFT calculation [126] was performed by assuming the stage 1 tilted structure. Consistent with the experimental results, the DFT study suggested that PF<sub>6</sub><sup>-</sup> preferentially migrates along the <100> direction with an estimated energy barrier of 0.23 eV.

Fast ion transport is conducive to high rate capability in rechargeable battery operation. Based on first principle calculations, Han *et al.* [121] reported that graphitic foam, characterized by good mechanical flexibility of few-layered graphene nanomaterials, played a key role for the ultrafast AIB. They found that the nanoscale thickness is mainly responsible for the observed ultrafast rate capability of graphitic foam. Specifically, the diffusivity of AlCl<sub>4</sub><sup>-</sup> increased dramatically once graphene film is less than five layers thick and found that the film thickness of four, three, and two graphene layers enables 48, 153, and 225 times enhanced diffusivity than that of the bulk graphite, respectively. The faster anion conductivity with the reduced film thickness is attributed to high elasticity of few-layered graphene, which provides more space for facile AlCl<sub>4</sub><sup>-</sup> diffusion as well. This study indicated that even bulky polyanions can be adopted as carrier ions for ultrahigh rate operation if highly elastic few-layered graphene is used as the active material.



## 2.5 Factors on the electrochemical performance of the batteries with anion intercalation graphite cathode

### 2.5.1 Solvent and operation voltage window

In batteries with anion intercalation graphite cathode, the electrolyte should be liquid [44, 47, 107, 116] or semi-solid gel [127], which is similar to LIBs. The safe voltage window of the electrolyte is determined by the lowest unoccupied molecular orbital (LUMO) and the highest occupied molecular orbital (HOMO) [128]. The electrochemical potentials of the anode ( $\mu_a$ ) and the cathode ( $\mu_c$ ) should match the LUMO and HOMO of the electrolyte to avoid electrolyte decomposition. For the anion intercalation cathode, the anions intercalation occurs at quite high potentials [110, 129-131]. Therefore, searching for suitable electrolytes which maintain stable operation at high potential is of significant necessity.

Ji *et al.* [51] proposed that, without considering the entropy change during the charge process of the cell, the free energy change  $\Delta G$  of the cathode//Li half-cell, can be described by the **Equation (3)**, where  $E(C^+A^-)$  is the energy of the charged cathode with an anion inserted,  $E(C)$  is the energy of the cathode before intercalation,  $E(Li)$  is the cohesive energy of Li metal for the addition of one lithium atom,  $\Delta H$  (*desolv.* of  $Li^+$ ) and  $\Delta H$  (*desolv.* of  $A^-$ ) are the desolvation energies of  $Li^+$  cations and anions from the electrolyte. This equation suggests that the operation potential of the cathode is related to the identities of the cathode and the lattice energy of the  $C^+A^-$  “salt”, as well as the solvents used in the electrolyte.

$$\Delta G = -eV \approx \Delta H = E(C^+A^-) - E(C) + E(Li) + \Delta H(\text{desolv. of } Li^+) + \Delta H(\text{desolv. of } A^-) \quad (3)$$

Placke *et al.* [114] studied the discharge capacity and the coulombic efficiency (CE) at varying

upper charging end potentials ranging from 4.8 V to 5.2 V vs. Li/Li<sup>+</sup> and it is found that these varying conditions leading to a discharge capacity increasement from 43 mAh g<sup>-1</sup> to 99 mAh g<sup>-1</sup>. However, the increase of the upper cut-off potential also led to a decrease of the CE. There are mainly two reasons: firstly, the high oxidizing potential the anion needed to intercalate into the graphitic cathode (usually above 4.5 V vs. Li/Li<sup>+</sup>), in combination with the instability of organic solvents, which resulted in strong electrolyte degradation; secondly, the co-intercalation reactions of organic solvent into graphite can cause graphite exfoliation.

### 2.5.2 Salt type or anion size

The feasible electrolytes for DIBs contain anions including perchlorate (ClO<sub>4</sub><sup>-</sup>), tetrafluoroborate (BF<sub>4</sub><sup>-</sup>), PF<sub>6</sub><sup>-</sup>, AlCl<sub>4</sub><sup>-</sup>, TFSI<sup>-</sup>, bis (fluorosulfonyl) amide (FSA<sup>-</sup>) and cations including Li<sup>+</sup>, Na<sup>+</sup>, tetraethylammonium (Et<sub>4</sub>N<sup>+</sup>), 1-ethyl-3-methylimidazolium (EMI<sup>+</sup>), 1-butyl-1-methylpiperidinium (PP<sub>14</sub><sup>+</sup>), and 1,2-dimethyl-3-propylimidazolium (DMPI<sup>+</sup>)[51, 99, 132-140]. Salts, which is solid in the room temperature, are dissolved in organic solvent to compose a electrolyte (organic electrolyte) for DIBs; while salt which is liquid in the room temperature could be used directly as electrolyte (ionic liquid electrolyte) [141, 142].

Since DIBs works by the intercalation of anions into the graphitic materials, the salt type and anion size are of particular importance. While for AIBs, only AlCl<sub>4</sub><sup>-</sup> anion is involved and thus the size effect of the anion is not discussed here [44].

Most DIBs comprise a graphite cathode and a metal-ion insertion anode in a nonaqueous electrolyte [51, 99]. Anions solvated in nonaqueous electrolyte are usually polyatomic, such as ClO<sub>4</sub><sup>-</sup>, AsF<sub>6</sub><sup>-</sup>, PF<sub>6</sub><sup>-</sup>, and SbF<sub>6</sub><sup>-</sup>, which all are much bigger than the layer distance of graphite in size [43-48,

107]. As the radiuses of most potential anions are larger than the layer distance of the intercalation guests, some researchers proposed that anions with smaller radius are easier to reversibly intercalate into graphite. However, in the recently reported work [132], it was indicated that the electrolyte effects ion pair formation and self-aggregation but not anion size were the main reasons affecting the onset potential for anion uptake. On the other hand, high salt concentration can reduce the potential required for anion intercalation into the graphite cathode [44].

### **3. The application of anion intercalation cathode in aluminum ion batteries**

Rechargeable aluminum based battery is of particular attraction since it can offer considerable advantages of high anode capacity, safety and cost-effectiveness, due to the ultrahigh theory capacity of 2978 mAh g<sup>-1</sup> and 8034 mAh L<sup>-1</sup>, low-cost and incombustible nature of aluminum (Al) metal anode [52, 98, 100, 103, 143-147]. Nevertheless, the major challenge for aluminum-ion battery (AIB) resides in cathode material, which only exhibited low discharge potential (less than 1.2 V) without discharge voltage plateaus, low current density (less than 1 A g<sup>-1</sup>) and short cycle life (<100 cycles, capacity retention < 90%) with rapid capacity decay in previous reports [83, 84, 102, 103, 148]. As a result, despite the research over 30 years, AIBs is still not competitive with other battery system.

#### **3.1 The rise of AIBs with anion intercalation cathode**

Recently, Lin *et al.* [104] opened a new way for AIBs with excellent electrochemical performance. This new type of AIBs employ aluminum metal as the anode, AlCl<sub>3</sub> : [EMIM]Cl (1.3:1 mole ratio) as the electrolyte and a three-dimensional flexible and conductive interconnected

graphene networks as cathode (**Figure 4b**) [149]. The cell configuration and working mechanism are elaborated in **Figure 4a**.

During the charge of the battery, Al is deposited accompanying with the release of  $\text{AlCl}_4^-$  species on the metal anode and the intercalation of  $\text{AlCl}_4^-$  species on the graphite cathode; during the discharge of the battery, Al is dissolved with the formation of  $\text{Al}_2\text{Cl}_7^-$  species in the anode and the  $\text{AlCl}_4^-$  is released at the cathode. The overall electrochemical process involves the reversible deposition/dissolution of Al from the metal anode, and the intercalation/ de-intercalation of  $\text{AlCl}_4^-$  in the graphite cathode (**Figure 4a**). The cell prototype delivers a reversible capacity of approximately  $65 \text{ mAh g}^{-1}$  based on the cathode mass. Then, they testify that the intercalation species in graphite consists of both Al and Cl by means of X-ray photoelectron spectroscopy (XPS) and Auger electron spectroscopy (AES). In addition, the analysis of the peak separation by ex situ XRD patterns suggests a stage 4 graphite intercalation compound with an intercalant gallery height were intercalated between graphene layers in a distorted state. The prototype reveals a rather stable cycle life (200 cycles) at a current density of  $66 \text{ mA g}^{-1}$  without capacity fading and with an average cell voltage of about 2 V (**Figure 4c**). Furthermore, the electrolyte offers the key to the success of long cycling AIBs. The electrochemical intercalation of  $\text{AlCl}_4^-$  within graphite was initially demonstrated using molten salt (MCl- $\text{AlCl}_3$ ) at  $175 \text{ }^\circ\text{C}$  as the electrolyte, then reported operating at room temperature, using  $\text{AlCl}_3$ :1,2-dimethyl-3-propylimidazolium chloride (1.5:1 mole ratio) as electrolyte[52]. Later,  $\text{AlCl}_3$  : [EMIM]Cl (1.3:1 mole ratio) was utilized as suitable electrolyte. And it has been evidenced that the use of electrolyte with reduced water content improves the round trip CE. Finally, performance comparable with supercapacitors has been obtained ( $40 \text{ Wh Kg}^{-1}$ ) using a three-dimensional (3D) graphitic foam as cathode, along with no obvious capacity fading after 7500

cycles at the current density of  $4000 \text{ mA g}^{-1}$ .

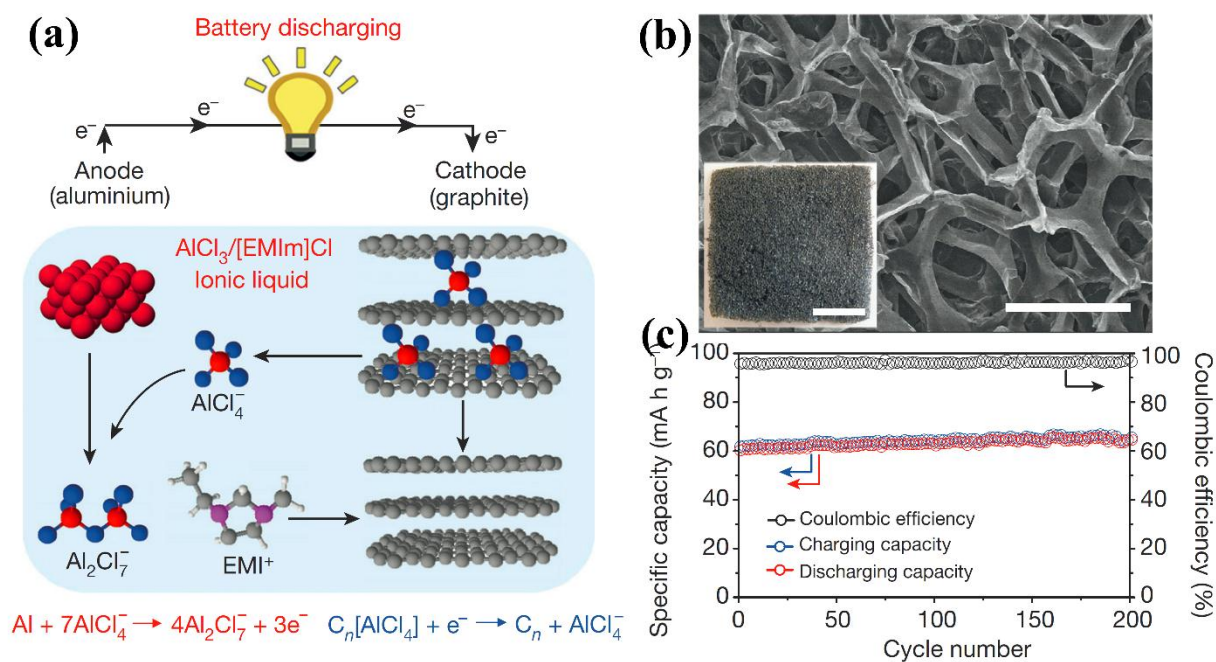


**Figure 4.** a) Schematic drawing of the Al/graphite cell during discharge, using the optimal composition of the  $\text{AlCl}_3/[\text{EMIm}]\text{Cl}$  ionic liquid electrolyte. On the anode side, metallic Al and  $\text{AlCl}_4^-$  were transformed into  $\text{Al}_2\text{Cl}_7^-$  during discharging, and the reverse reaction took place during charging. On the cathode side, predominantly  $\text{AlCl}_4^-$  was intercalated and de-intercalated between graphite layers during charge and discharge reactions, respectively; b) A scanning electron microscopy image showing a graphitic foam with an open frame structure; scale bar, 300 nm. Inset, photograph of graphitic foam; scale bar, 1 cm; c) Long-term stability test of an Al/PG cell at  $66 \text{ mA g}^{-1}$  [104]. Copyright (2015) Springer Nature.

Graphite or, more in general, carbon-based materials represent suitable candidates as cathode materials for aluminum cells [150]. And the development of novel graphite electrode is an important direction for high performance AIBs. Dai group [151] synthesized porous graphitic materials with vertically aligned graphene sheets with low density of defects or oxygen groups oriented perpendicular to a current collector substrate (**Figure 5a**), which was used as the cathode for AIBs. This AIB shows a discharge capacity of  $\sim 60 \text{ mAh g}^{-1}$  at a high current charge/discharge density up to

12 000 mA g<sup>-1</sup> stably cycled over 4000 cycles (**Figure 5b**). The high rate capability of this battery is partially originated from the enlarged interlayer spacing distance between graphene layers of cathode, within which the AlCl<sub>4</sub><sup>-</sup> diffusion becomes more favorable ascribed to lower migration energy barriers.

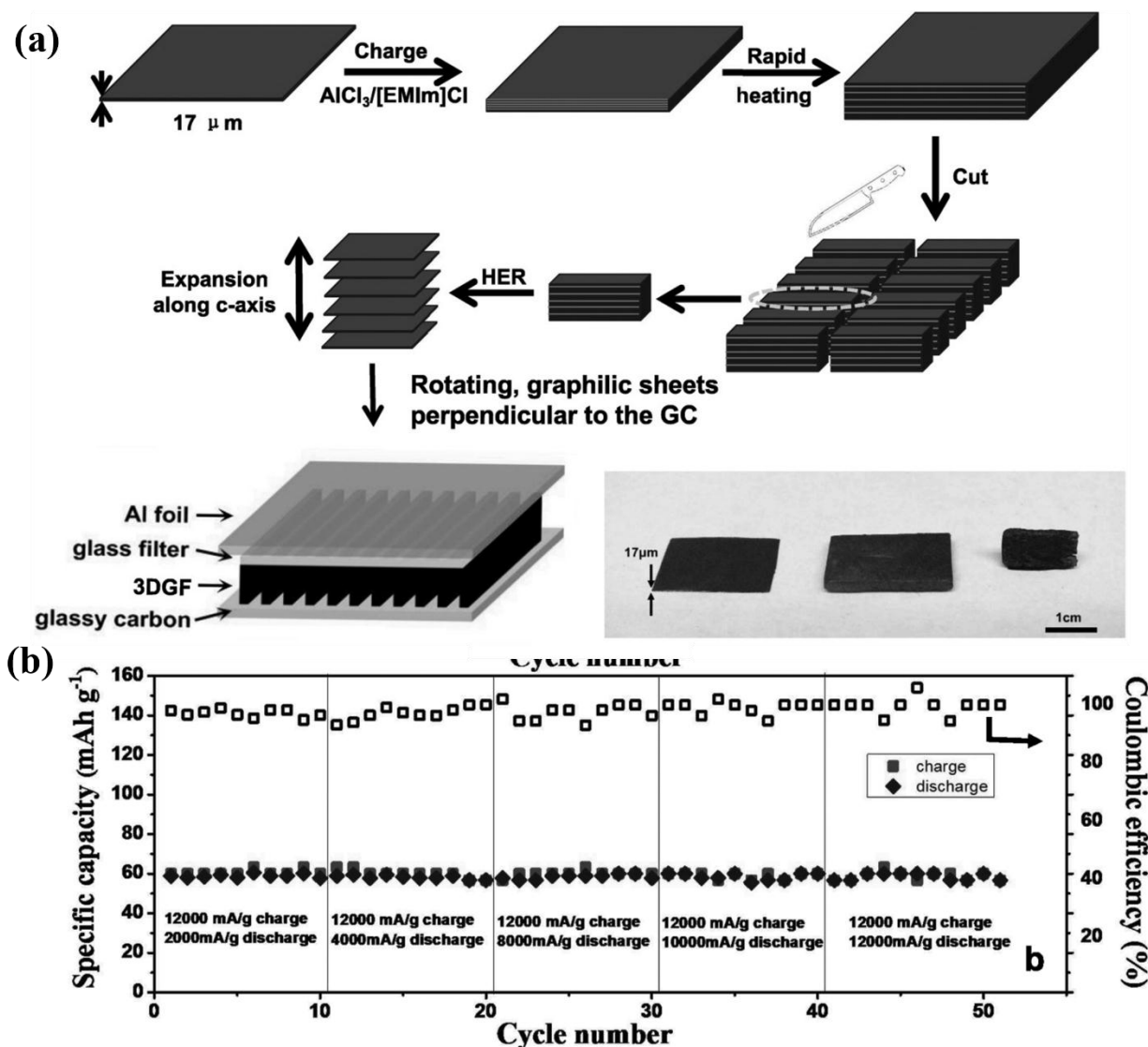


**Figure 5.** a) Schematic for the preparation of the 3D Graphitic Foam (3DGF) and the battery assembly. The inset shows the photograph of the pristine PG, first expansion PG and the 3DGF after second expansion; b) Galvanostatic charge and discharge curves of Al/3DGF cells charging at 12 000 mA g<sup>-1</sup> and discharging at various current densities ranging from 2000 to 12 000 mA g<sup>-1</sup> [151]. Copyright (2016) John Wiley and Sons.

### 3.2 The booming of AIBs with anion intercalation cathode

Apart from the low capacity that limits the cell energy density, there remain two key challenges for AIB cathode: insufficient high-rate performance which causes cell power density inferior to supercapacitors and relatively low Columbic efficiency (CE).

To further increase the specific capacity of AIBs, Dai group [118] proposed an AIB cell using pristine natural graphite (NG) flakes, which achieves a much higher specific capacity of  $110 \text{ mAh g}^{-1}$  with CE of 98%, at a current density of  $99 \text{ mAh g}^{-1}$  (0.9 C), and clear discharge voltage plateaus (2.25–2.0V and 1.9–1.5 V). They investigated various graphite materials for AIB cathodes and found that NG was superior to synthetic graphite (KS-6 and MCMB) in contributing to higher capacities and well-defined voltage plateaus. They studied Raman and X-ray diffraction data and attributed the lower capacity and less distinguished discharge voltage plateaus of KS-6 and MCMB materials to their higher surface areas, lower crystallinities and higher defect densities than NG. These results indicated that suitability of high crystallinity, low defect density graphite materials is necessary for use in high-performance AIB.

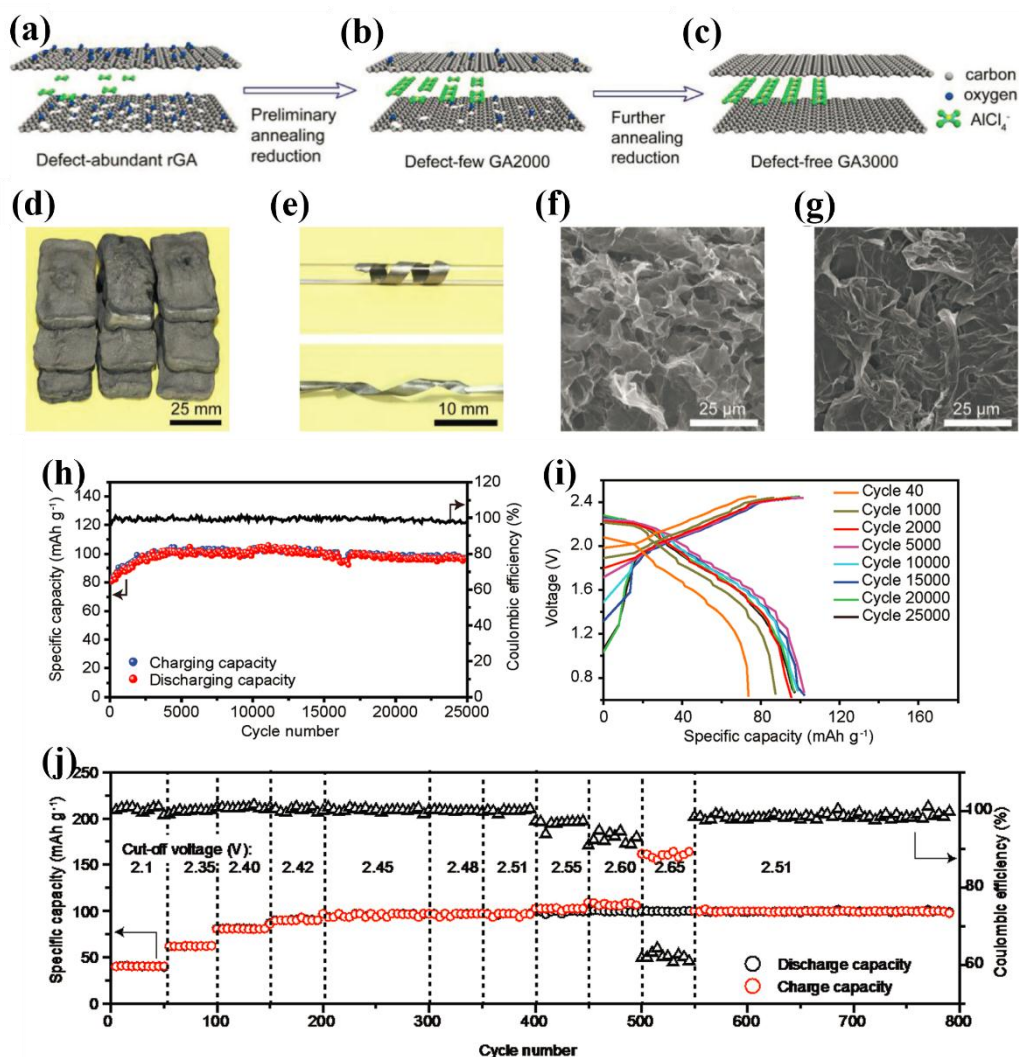


Figure 6. Design and production of GA cathode. a–c) Schematic of the defect-free design. Defects ( $sp^3$  carbons and oxygen-containing groups) in a) rGA and b) GA-2000 reduce the electrical conductivity, impede the transportation of  $AlCl_4^-$  and cannot act as active sites; c) the defect-free  $sp^2$  carbon networks in GA-3000 act as active sites and facilitate the transportation of  $AlCl_4^-$ . d) Digital camera image of GA-3000. e) A compressed GA-3000 strip is coiled around a glass rod to illustrate the good flexibility and twisted by two tweezers to show the twistability. f,g) SEM images of f) GA-3000 and g) compressed GA-3000 paper; h) Galvanostatic cycling of GA-3000 ( $5\text{ A g}^{-1}$ ) over 25 000 cycles. i) Detailed charge and discharge curves of GA-3000 cathode at different cycles (50 C). j) The specific capacity and CE of GA-3000 cathode at different cutoff voltage [152]. Copyright (2017) John Wiley and Sons.



The above AIB with NG flakes as cathode show a higher specific capacity, but the rate capability is poor. To improve the rate property of AIBs, Gao's group [152] proposed a defect-free principle to design graphene based cathode. This cathode was made from with highly crystallized defect-free few-layer graphene aerogel (GA) (**Figure 6a-g**), and as a result, this defect-free cathode with completely crystallized  $sp^2$  carbons in GA's atomic structure, leads to improved rate performances of AIB (e.g.,  $100 \text{ mAh g}^{-1}$  at  $5 \text{ A g}^{-1}$ ,  $97 \text{ mAh g}^{-1}$  at  $50 \text{ A g}^{-1}$ ) (**Figure 6h-j**). Excellent electrochemical performance with defect-free cathode should be mainly due to three advantages: (1) elimination of inactive defects facilitating the fast intercalation of large-sized anions and simultaneously providing more active sites for energy storage; (2) greatly enhanced electrical conductivity recovering defective graphene into electrical highway; and (3) high reproducibility of material quality and cell performance favoring large scale manufacture.

To further promote the cycle life and rate capability of the AIBs, the same group [153] propose a "trihigh tricontinuous (3H3C) design" to achieve the ideal graphene film (GF-HC) cathode with excellent electrochemical performances. Ordered assembly of graphene liquid crystal with a highly oriented structure can satisfy the requirement of high mechanical strength and Young's modulus for preventing material collapsing or disintegrating during repeated anion intercalation and de-intercalation. High temperature annealing and concomitant "gas pressure" contributed to high-quality yet high channeling graphene structure that met requirements: (1) highly crystallized defect-free graphene lattice as active anion intercalation site affording available energy storage capacities; (2) continuous electron-conducting matrix for large current transportation and internal polarization mitigation; and (3) interconnected channels facilitating high electrolyte permeability, ion

diffusion, and further fast redox reaction between electrolyte and active material. Owing to the targeted “3H3C design”, the resulting aluminum-graphene battery (Al-GB) achieved ultra-long cycle life (91.7% retention after 250,000 cycles), unprecedented high-rate capability ( $111 \text{ mAh g}^{-1}$  at  $400 \text{ A g}^{-1}$  based on the cathode), wide operation temperature range ( $-40 \text{ }^\circ\text{C}$  to  $120 \text{ }^\circ\text{C}$ ), unique flexibility, and non-flammability.

Graphene is an important basic unit in the bottom-up preparation of graphite cathode. To clarify the influence factor of plane size and stacking layer number of graphene, Liu *et al.*[154] demonstrated that the size of graphitic material in ab plane and c direction in anion intercalation chemistry. Sharply decreasing the size of vertical dimension (c direction) strongly facilitates the kinetics and charge transfer of anions intercalation and de-intercalation. On the other hand, increasing the size of horizontal dimension (ab plane) contributes to improving the flexibility of graphitic materials, which results in raising the cycling stability. Meanwhile,  $\text{AlCl}_4^-$  are reversibly intercalated into the interlayer of graphite materials, leading to the staging behaviors (**Figure 7**). Large horizontal dimension-small vertical dimension graphite can undergo massive cycles of anions (de)intercalation at both low and high current densities without any structural damages. On the contrary, small horizontal dimension-small vertical dimension graphite can be easily stripped off by anions intercalation after a long-time cycling.

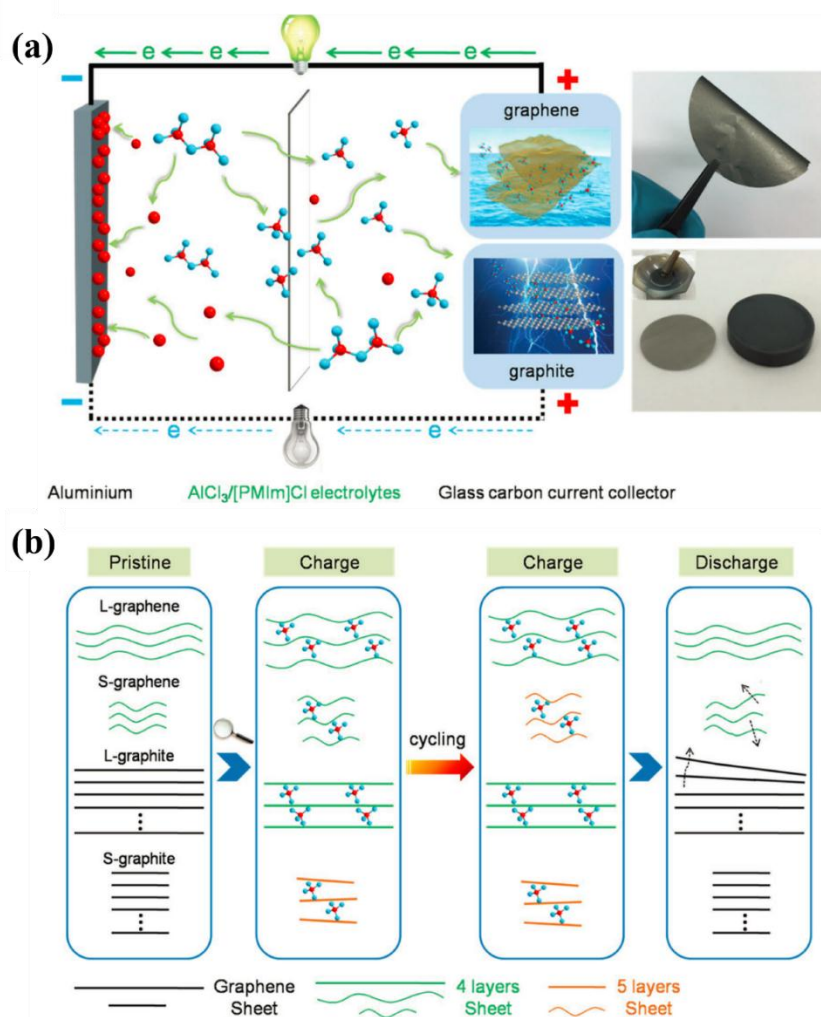


**Figure 7.** a) Schematic of Al-graphene and Al-graphite batteries (left). Photographs of graphene and graphite electrode (right): the size of steel mesh is 13 mm. b) Schematics of aluminum-ion intercalation chemistry in graphene and graphite electrodes [154]. Copyright (2017) John Wiley and Sons.

**Table 1.** AIB systems and electrical performance of reported results.

Ref	Cathode	Anode	Electrolyte	Voltage region	Specific capacity	Cycling capability
[151]	Exfoliated graphite	nickel foils	$\text{AlCl}_3$ to [EMIm]Cl = 1.3.	1.8 V	$\approx 60 \text{ mAh g}^{-1}$	$60 \text{ mAh g}^{-1}$ at 12 000 mA $\text{g}^{-1}$ 4000 cycles
[104]	3D Graphitic Foams	Al foil	$\text{AlCl}_3$ to [EMIm]Cl = 1.3.	$\sim 2.0$ V	$65 \text{ mAh g}^{-1}$ $5,000 \text{ mA g}^{-1}$ (75C) $\sim 60 \text{ mAh g}^{-1}$	$\sim 100\%$ after 7500 cycles
[152]	Graphene	Al foil	$\text{AlCl}_3$ to [EMIm]Cl	50 C	$95 \text{ mAh g}^{-1}$ at 5 C, 10 C,	97% after 25 000 cycles

			= 1.3.	1.95V	and 20 C	
				0.5-2.51 V	100 mAh g <sup>-1</sup> at 30 C	
					100 mAh g <sup>-1</sup> at 50 C	
					100 mAh g <sup>-1</sup> at 100C	
					97 mAh g <sup>-1</sup> at 200 C	
					97 mAh g <sup>-1</sup> at 500 C	
[118]	natural graphite	Al foil	AlCl <sub>3</sub> to [EMIm]Cl = 1.3.	0.5-2.45 V	110 mAh g <sup>-1</sup> at 99 mA g <sup>-1</sup> (0.9C)	60 mAh g <sup>-1</sup> at 6C, over 6,000 cycles
[153]	GF-HC	Al foil	AlCl <sub>3</sub> to [EMIm]Cl = 1.3.	0.5-2.50 V	120 mAh g <sup>-1</sup> at 6 A g <sup>-1</sup> 111 mAh g <sup>-1</sup> at 400 A g <sup>-1</sup>	91.7% after 25 000 cycles

### 3.3 The challenges of AIBs with anion intercalation cathode

Above mentioned work (**Table 1**) have developed powerful cathode to improve the performance of AIBs. However, there is still a lot of space for further improvement of the AIBs. Firstly, the CE about 97–98% obtained for this battery is lower than those of state-of-the-art LIBs, the CE of which can reach up to 99.98%, a benchmark that should be also achieved by alternative battery systems. Hahn *et al.* [146] studied the overall cycling behavior upon different rate, revealing a satisfactory CE at higher rate. And they conferred the higher CE upon increasing currents were ascribed to the kinetic limitation of the side reactions. Later, Dai group improved the CE to ~99.7% with urea added into the electrolyte [117].

Another consideration is that current existed AIB uses 1-ethyl-3-methylimidazolium chloride (EMIC) as electrolyte, which is relatively expensive. New electrolytes for this system could include any which are capable of reversible aluminum deposition/dissolution. Thus, Angell *et al.* [117] investigate the performance of a rechargeable Al battery using a modified electrolyte with urea as electrolyte additive, which shows a high CE (~99.7%), a lower cost (~50 times cheaper than EMIC) and a higher eco-friendliness.

Furthermore, the energy density of the AIB (40 Wh kg<sup>-1</sup>) makes it not suitable for high energy

applications, such as electric vehicles. DIBs, operating at higher voltage than AIBs, are coming into sight.

## 4. The application of anion intercalation cathode in dual-ion batteries

In DIBs, the ions are supplied by the electrolyte rather than anode or cathode. Thus, the solvent, salt type and salt concentration of the electrolyte are critical factors for the DIBs' performance. In addition, the electrolyte must be considered as a part of the active mass.

### 4.1 DIBs based on lithium ion electrolyte

#### 4.1.1 Graphite cathode-metal oxide anode DIBs

By using graphite as the cathode and  $\text{MoO}_3$  as the anode, a novel DIB was initially reported by Yoshio *et al.* [155]. The cell worked by the intercalation and de-intercalation of  $\text{PF}_6^-$  in the cathode (graphite) and conversion process of  $\text{Li}^+$  in the anode ( $\text{MoO}_3$ ). This cell (the weight ratio of cathode to anode material is 1:1 and the electrolyte concentration) configuration demonstrated an initial discharge capacity of  $81 \text{ mAh g}^{-1}$ , which remains 90% capacity retention from 3rd to 200th cycles and the overall voltage region of graphite/ $\text{MoO}_3$  located in the range of 1.5-3.5 V (using a 1.0 M  $\text{LiPF}_6$  solution as the electrolyte). They suggest that performance of this energy storage system could be improved by changing the weight ratios of the cathode to anode and the concentration of the electrolyte. Similarly, Yoshio *et al.* [111] also developed a DIB system employing KS-6 graphite cathode and niobium oxide ( $\text{Nb}_2\text{O}_5$ ) anode with a 1:1 weight ratio of cathode to anode. The cell, with a voltage range of 1.5-3.5 V, delivered 57 and 26  $\text{mAh g}^{-1}$  at 1C and 35C rates, respectively. The DIB systems above were inherently safe resulted from: 1) no oxygen is released from cathode materials, 2)

no lithium dendrite is formed at the anode (high lithium reaction potential), and 3) no possibility of overcharge from the electrode/electrolyte reaction.

#### 4.1.2 Graphite cathode-graphite/reduced graphene-based anode DIBs

DIBs with metal oxide anode have a relatively high operation voltage with lithium ions, the lower reaction voltage of graphite and reduced graphene oxide would induce a higher operation voltage and thus beneficial to energy density [156]. A DIB system reported by Zheng *et al.* [130] used 1-Ethyl-3-methylimidazolium hexafluorophosphate ((EMIm)<sup>+</sup> (PF<sub>6</sub>)<sup>-</sup>) ionic liquid as the electrolyte, graphite as cathode, reduced graphene oxide (RGO) as anode. The cell chemistry was based on the intercalation of PF<sub>6</sub><sup>-</sup> anions into graphite as cathode reaction and the EMIm<sup>+</sup> adsorption onto the surface of RGO as negative electrode reaction. As this cell is a kind of hybrid capacitor and the specific capacitance is only ~30 F g<sup>-1</sup>, the energy density is relative low (70 Wh kg<sup>-1</sup>). Pure 1-butyl-1-methylpiperidinium bis(trifluoromethylsulfonyl)imide (Pyr<sub>14</sub>TFSI), which has a high electrolyte window, exhibited a high discharge plateau initiated at 4.4 V, a well-defined capacity of 82 mA h g<sup>-1</sup>, an ultrawide charge/discharge potential range of 1.0-5.0 V and a superior stability of 100% capacity retention for 600 cycles [131].

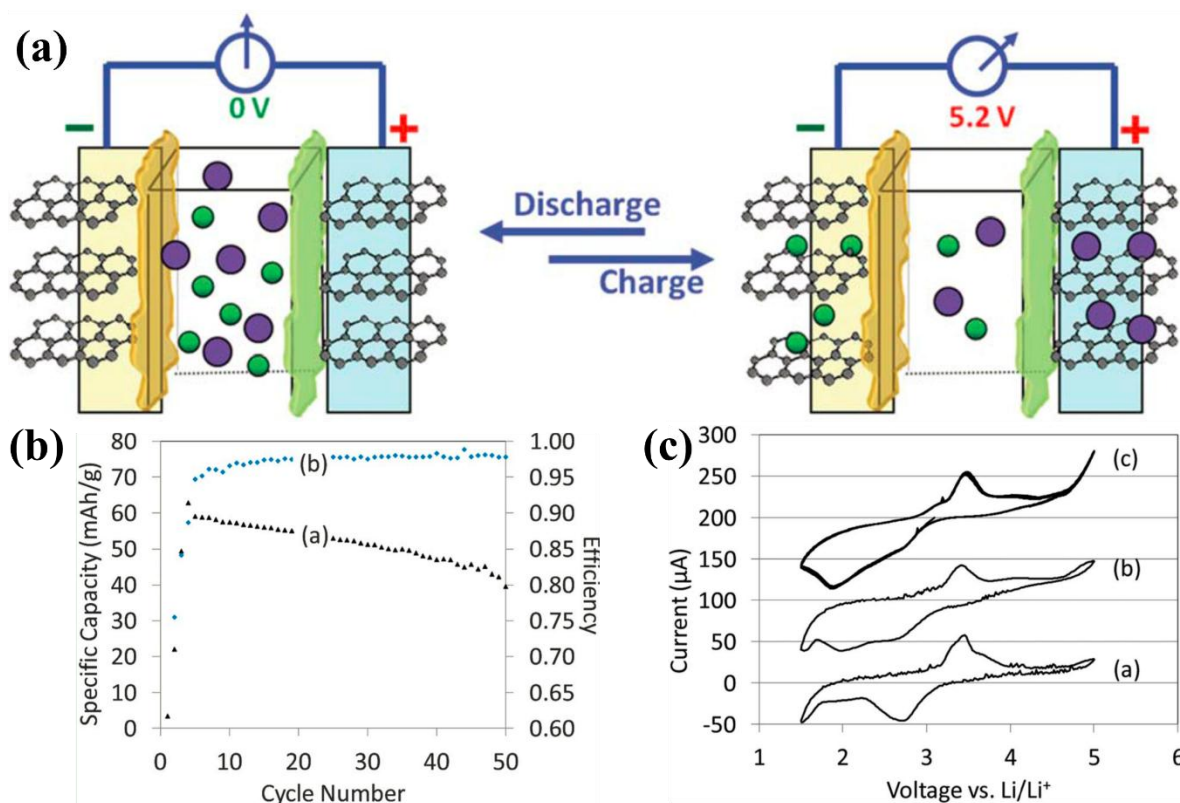


**Figure 8.** (a) Schematic illustration of a dual-graphite intercalation cell wherein Li<sup>+</sup> and PF<sub>6</sub><sup>-</sup> simultaneously accommodate in graphitic structures at the anode and cathode upon charge; (b) full cell cycling of dual-graphite cell (inset a) specific capacity (mAh g<sup>-1</sup>) and (inset b) efficiency; (c) cyclic voltammograms of a lithium/platinum sense cell embedded in a lithium/graphite cell (inset a) before cycling, (inset b) during cycling and (inset c) at OCV after cycling shifted up progressively by 100 μA for clarity [81]. Copyright (2013) Royal Society of Chemistry.

Read *et al.* [81] enabled a reversible dual-graphite intercalation chemistry with simultaneous accommodation of Li<sup>+</sup> and PF<sub>6</sub><sup>-</sup> in graphitic structures (the cathode was MCMB graphite and the anode graphite was “CPreme” from Conoco Phillips) by a high voltage electrolyte based on a fluorinated solvent and additive, which is capable of supporting at the electrochemical window up to 5.2 V with high efficiency (**Figure 8**). However, the understanding as to structure of the anion intercalate formed in these electrolyte systems and the effect of solvent co-intercalation on cathode performance are still limited. This effort was undertaken by Read using a number of in situ

techniques to better characterize the fully intercalated composition as well as to investigate the process of solvent co-intercalation. Read [157] has shown that solvent molecules move with anion during the intercalation/de-intercalation process while analysis of fully intercalated crystals demonstrated that there is an unusually strong preference for ethyl-methyl carbonate (EMC) over fluoroethylene carbonate (FEC) to co-intercalate in this anion intercalation compound. Almost at the same time, Winter and Placke *et al.* [82] reported dual-graphite cells (CG graphite as anode and KS6L graphite as cathode) (**Figure 9**) based on the reversible intercalation of TFSI from an ionic liquid electrolyte and also showed high specific capacity of  $97 \text{ mAh g}^{-1}$ .

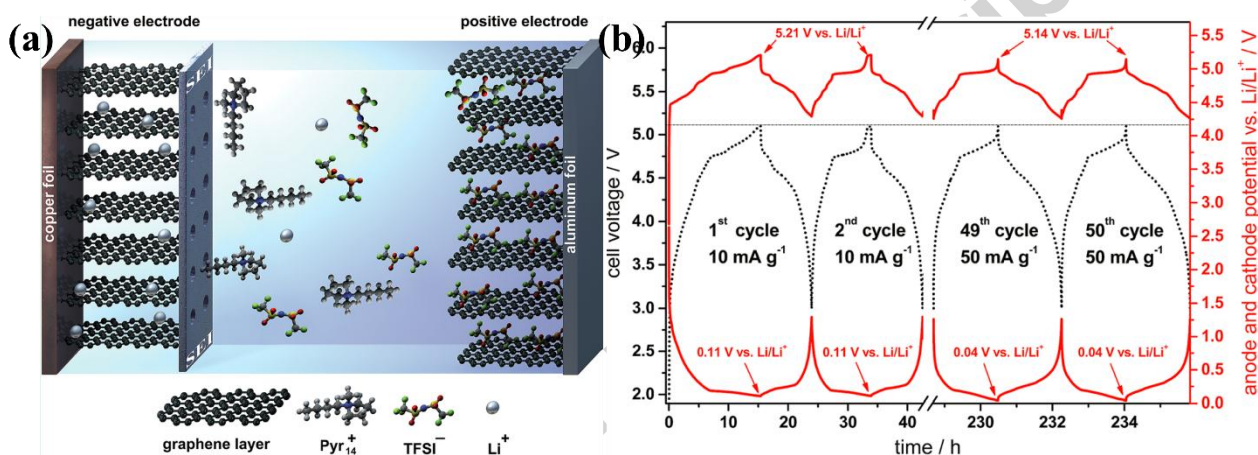


**Figure 9.** (a) Schematic illustration of a dual-graphite cell with an effective SEI layer at the graphite anode during the charge process. The negative graphite electrode is protected from co-intercalation reactions of pyrrolidinium cations by the SEI layer; the SEI still allows the transport and intercalation of lithium ions; (b) cell voltage vs. time profile (black, dotted curve) and anode and cathode potential vs. time profiles (red curves) of the CG/KS6L dual-graphite cell during representative cycles of the constant current charge/discharge cycling process. The specific current for cycles 1–3 is  $10 \text{ mA g}^{-1}$  and  $50 \text{ mA g}^{-1}$  for the following cycles. Cell voltage range: 3.0 V and 5.1 V [82].



## 4.1.3 Graphite cathode- metal anode DIBs

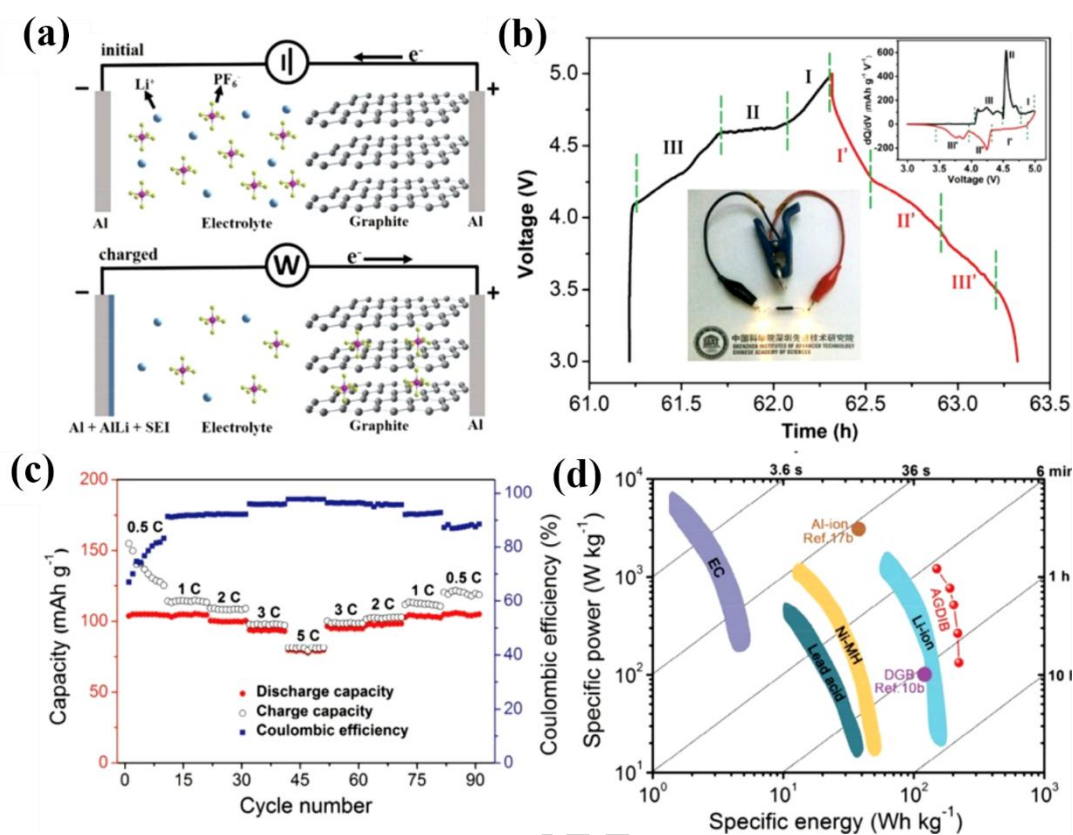


**Figure 10.** (a) Schematic illustration of the working mechanism of AGDIB. (b) Galvanostatic charge/discharge performance of the AGDIB at 0.5 C in 4M  $\text{LiPF}_6$ /(EMC + 2% VC). Insets are the  $dQ/dV$  curves of this battery and a digital photograph showing that a single AGDIB lighted up two yellow LEDs in series. (c) Rate capacities and corresponding CE of obtained AGDIB. (d) Cell performance of AGDIB in comparison to conventional energy storage devices with state of the art properties [158]. Copyright (2016) John Wiley and Sons.

For the first time, Tang group reported a novel concept of aluminum-graphite DIB (AGDIB) [158] by using Al foil as both anode and current collector, graphite as cathode and 4 M  $\text{LiPF}_6$  in EMC as electrolyte. The working mechanism of the AGDIB is schematically illustrated in **Figure 10**. Upon the charge process, the  $\text{Li}^+$  cations were extracted from the electrolyte and deposited on the Al anode to form an Al-Li alloy, while the  $\text{PF}_6^-$  anions were intercalated into the graphite cathode

simultaneously. The discharge process reversed, where both  $\text{Li}^+$  and  $\text{PF}_6^-$  diffused back into the electrolyte. As shown in **Figure 10b**, three distinctive regions of 4.08-4.59 V (stage III), 4.59-4.63 V (stage II) and 4.63-5.0 V (stage I) were found, corresponding to the anions intercalation stage of graphite. As shown in **Figure 10c**, the AGDIB displayed discharge capacities of 105, 104, 100, 93, and 79 mAh  $\text{g}^{-1}$  at 0.5, 1, 2, 3, and 5 C, respectively, and kept high reversibility with invariable capacities when the current rate was set back to lower values. At a high current density of 2 C, a capacity retention of 88% was achieved after 200 charge/discharge cycles, revealing good cycling stability. As shown in **Figure 10d**, the AGDIB was capable to deliver specific energy densities of  $\sim 222$  and  $150 \text{ Wh kg}^{-1}$  at power densities of 132 and  $1200 \text{ W kg}^{-1}$ , respectively, which were higher than commercial LIBs ( $\sim 200 \text{ Wh kg}^{-1}$  at  $50 \text{ W kg}^{-1}$ , and  $\sim 100 \text{ Wh kg}^{-1}$  at  $100 \text{ W kg}^{-1}$ ). The dramatic electrochemical performance was mainly resulted from the following reasons: (1) high concentration of lithium salt in the electrolyte; (2) effective electrolyte additive (2 wt% vinylene carbonate, VC) in the carbonate electrolyte as an SEI film formation agent to protect the anode to achieve good rate capability and stable cycling performance; (3) Al foil acted as both anode and current collector, which significantly reduce the dead weight and dead volume of the AGDIB, thus contributing to increased specific energy density and volume energy density.

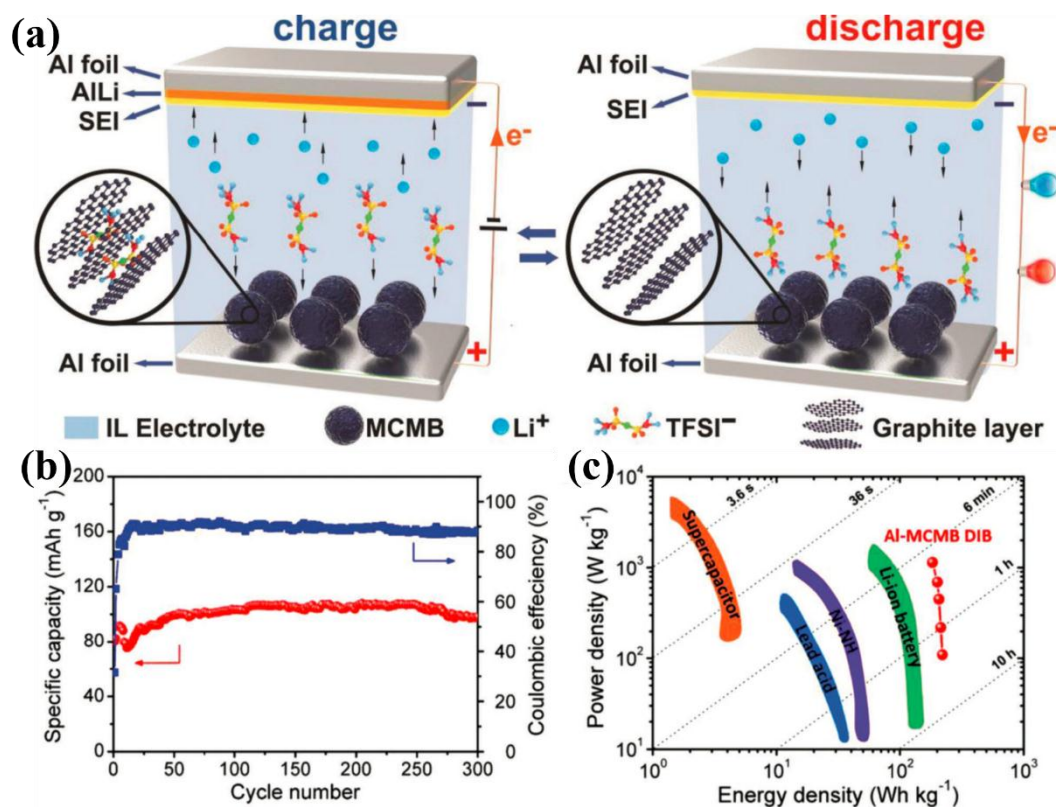


**Figure 11.** a) Schematic illustration of charge/discharge processes of the dual-ion battery using Al foil as anode and MCMB as cathode based on an ionic liquid electrolyte. b) Long-term cycling performance of the battery at 0.5 C for 300 cycles. c) Ragone plot of the Al-MCMB DIB compared with conventional energy storage devices [159].

Copyright (2016) John Wiley and Sons.

Subsequently, the same group utilized a lithium-salt containing ionic liquid (1 M LiTFSI in Pyr<sub>14</sub>TFSI and 10% FEC) [159] as the electrolyte to further increase the cycling stability, since the ionic liquid is more stable than organic electrolyte under high operating voltage. DIB using MesoCarbon MicroBeads (MCMB) as cathode and Al foil as anode with an ionic liquid electrolyte has demonstrated superior cycling stability with a reversible capacity of 98 mAh g<sup>-1</sup> after 300 cycles at 0.5 C (**Figure 11**).

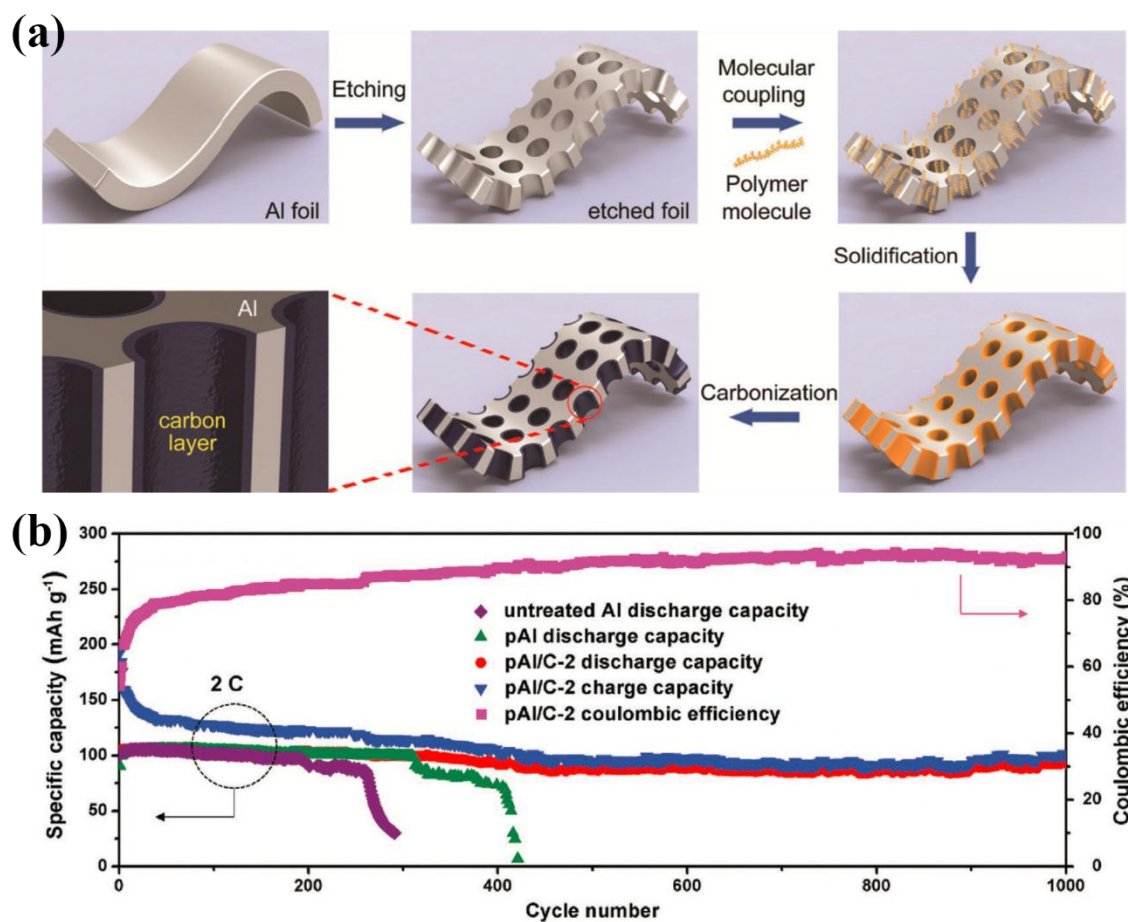


**Figure 12.** (a) Schematic illustration of the fabrication process to make the pAl/C anode material; (b) long-term cycling performance of the pAl/C-G DIB at 2 C for 1000 cycles with pAl and untreated Al foil as controls [160].

Copyright (2016) John Wiley and Sons.

The stability of Al anode in AGDIB is of high importance for long cycling life, as Al anode will suffer from huge volume variation during lithium alloying and de-alloying. Accordingly, Tang group developed a carbon-coated 3D porous aluminum (pAl/C) anode [160], which can efficiently alleviate the mechanical stress caused by alloying process between Al and Li, and also promote the ion diffusion efficiency for enhanced rate performance. Furthermore, the carbon out-layer can also help buffer the anode volume change, and passivate undesirable reactions on Al surfaces. Due to the synergistic effects, the DIB made from pAl/C showed superior electrochemical performances including high stability with 89.4% capacity retention after 1000 cycles at 2 C and ideal rate

performance with 81.7% capacity retention at 20 C compared to that at 2 C (**Figure 12**). As for the interfacial modification, Tang group synthesized a carbon coated hollow aluminum nanospheres on Al foil as high-efficient anode material [161]. The hollow interface design can define the alloying/de-alloying position inside the hollow nanostructures, and thus effectively alleviate the surface pulverization and crack. The DIB based on carbon coated hollow nanospheres modified Al anode showed excellent cycling stability with 99% capacity retention after 1500 cycles (**Figure 13**). All of these demonstrations provide a new potential avenue for the potential industrialization of DIBs.

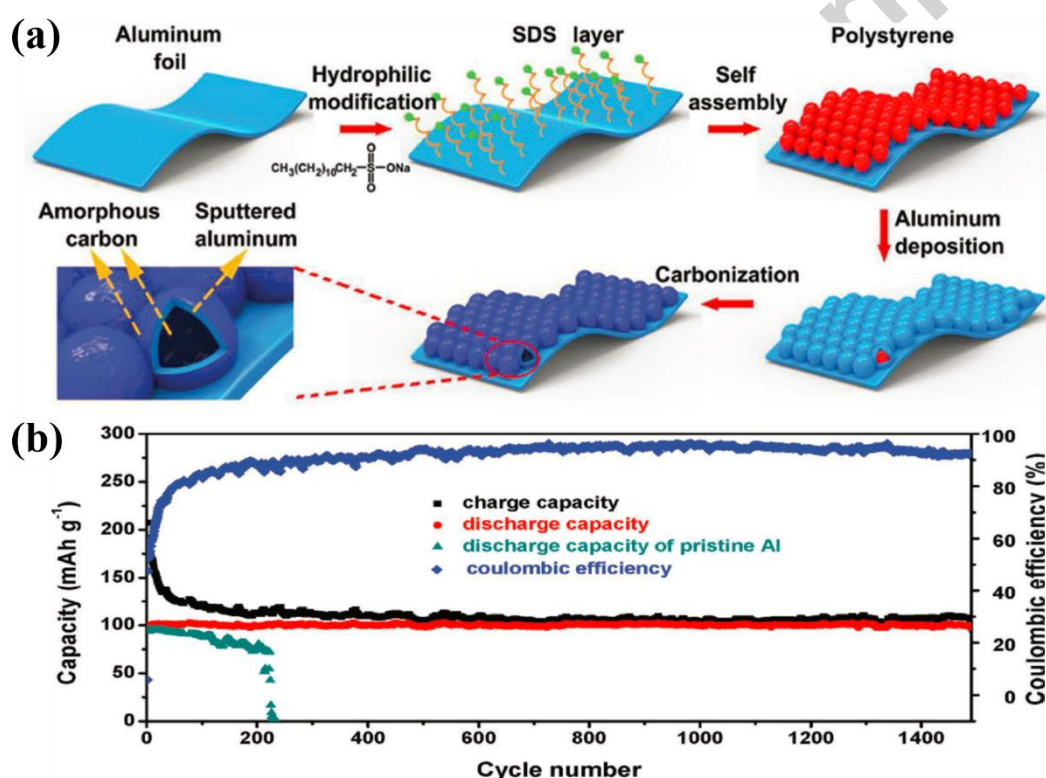


**Figure 13.** (a) Schematic illustration of the CHAA fabrication process for the DIB; (b) long-term cycling performance of the CHAA-DIB in comparison to the pristine Al foil-based DIB [161]. Copyright (2017) John Wiley and Sons.

More recently, Tang group [162] reported an integrated dual-ion battery design with active

materials, current collectors, and separator, assembled into one flexible component. An aluminum film was deposited directly onto one side of the 3D porous glass fiber separator to form a porous anode, and graphite cathode were loaded on the other side of the separator, along with aluminum film deposited on the top as current collector. This design demonstrates ultrafast charge/discharge rate up to 120 C while maintaining high capacity of 116.1 mA h g<sup>-1</sup>. Moreover, long-term stability of over 1500 cycles at a high rate of 60 C is achieved. The estimated energy density remains as high as 232.6 Wh kg<sup>-1</sup> at an ultrahigh power density of 22634.5 W kg<sup>-1</sup> (Figure 14).

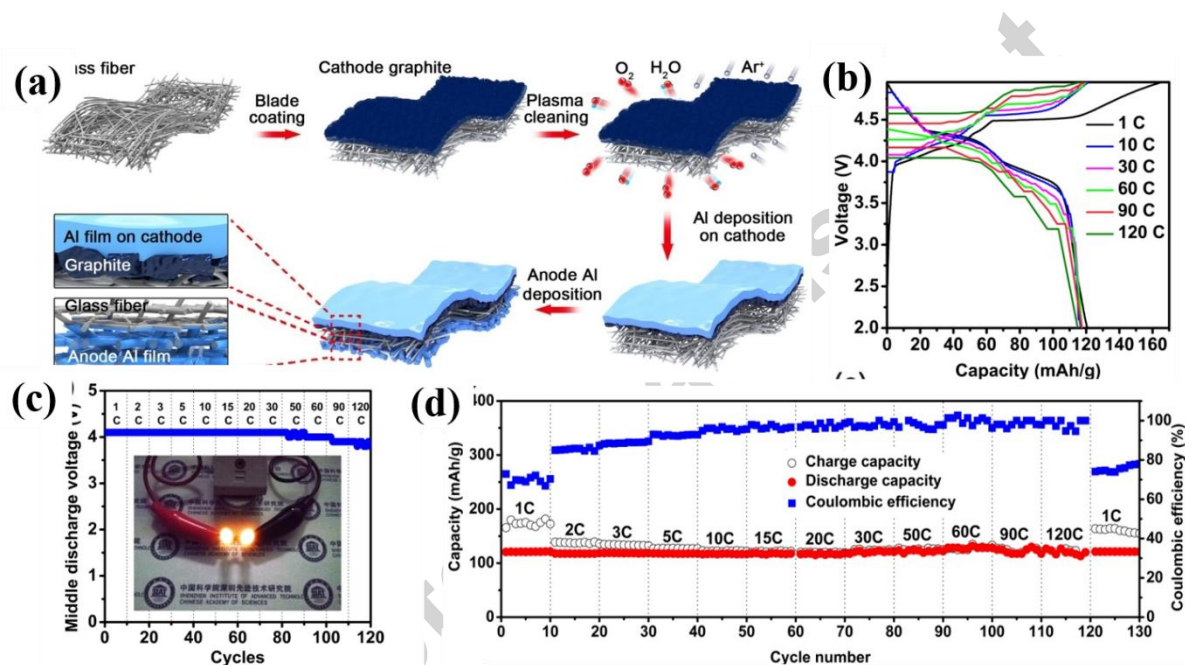


**Figure 14.** a) Schematic illustration of the preparation process of the integrated dual-ion battery (DIB). b) Charge–discharge curves and c) the middle discharge voltages of the integrated dual-ion battery (DIB) at different current rates ranging from 1 to 120 C. d) Rate capacities and corresponding CE of the integrated DIB at current rates ranging from 1 to 120 C [162]. Copyright (2017) John Wiley and Sons.

In addition, lithium metal is another kind of metal anode for DIBs. For example, Dai and Jin *et al.* [163] report a simple electrochemical route for the graphitization of amorphous carbons through cathodic polarization in molten CaCl<sub>2</sub> at temperatures of about 1100 K, which generates porous

graphite comprising flower-like nanoflakes. This nanostructured graphite allows fast and reversible intercalation/de-intercalation of anions, promising a superior cathode material for batteries. In a Pyr<sub>14</sub>TFSI ionic liquid and paired with a lithium metal anode, it exhibits a specific discharge capacity of 65 and 116 mAh g<sup>-1</sup> at a rate of 1800 mA g<sup>-1</sup> when charged to 5.0 and 5.25 V vs. Li/Li<sup>+</sup>, respectively. The capacity remains fairly stable during cycling and decreases by only about 8% when the charge/discharge rate is increased to 10000 mA g<sup>-1</sup> during cycling between 2.25 and 5.0 V.

## 4.2 Other metal ion based DIBs

Other metal, such as sodium [164], potassium [165, 166], aluminum [167], rather than lithium, based rechargeable ion batteries offer the possibilities for safety, high energy density and low cost (**Table 2**). For example, Lu *et al.* [167] developed an aluminum based high-rate capability dual-ion battery with an aluminum anode and a 3D graphene cathode. The battery operated by the electrochemical deposition and dissolution of aluminum at the anode, and intercalation/de-intercalation of ClO<sub>4</sub><sup>-</sup> anions in the graphene based cathode with a Al(ClO<sub>4</sub>)<sub>3</sub>/Propylene carbonate - fluoroethylene carbonate electrolyte. The battery exhibited plateaus (about 1 V), high-rate capacity (101 mA h g<sup>-1</sup> at 2000 mA g<sup>-1</sup>) and long cycle life (more than 400 cycles). More importantly, the battery also showed superior electrochemical properties with fast charge and slow discharge (the battery could be fully charged in 13 min and discharged for more than 73 min).

## 4.3 Hybrid anion DIBs

A hybrid battery, consisted of a dual-salt electrolyte with two types of anion or/and cation, can

exhibit excellent battery performances including long cycle life, fast charge/discharge rate, and high CE [44, 113, 168-177]. Jiao *et al.* presented a “multi-ions battery”, using graphite as the cathode and Al foil as the anode in a  $\text{LiPF}_6 + \text{AlF}_3$  EMC-DMC electrolyte, in combination with vinylene carbonate (VC) as a SEI-forming additive. The energy storage in this multi-ions battery is based on the intercalation of complex anions ( $\text{PF}_6^-$  and  $\text{AlF}_4^-$ ) into the graphite electrode, and the deposition of Li on the surface of the Al electrode to form an  $\text{AlLi}_x$  alloy during the charge process. During the discharge process, all ions are released into the electrolyte again. This process is illustrated schematically in **Figure 15**.

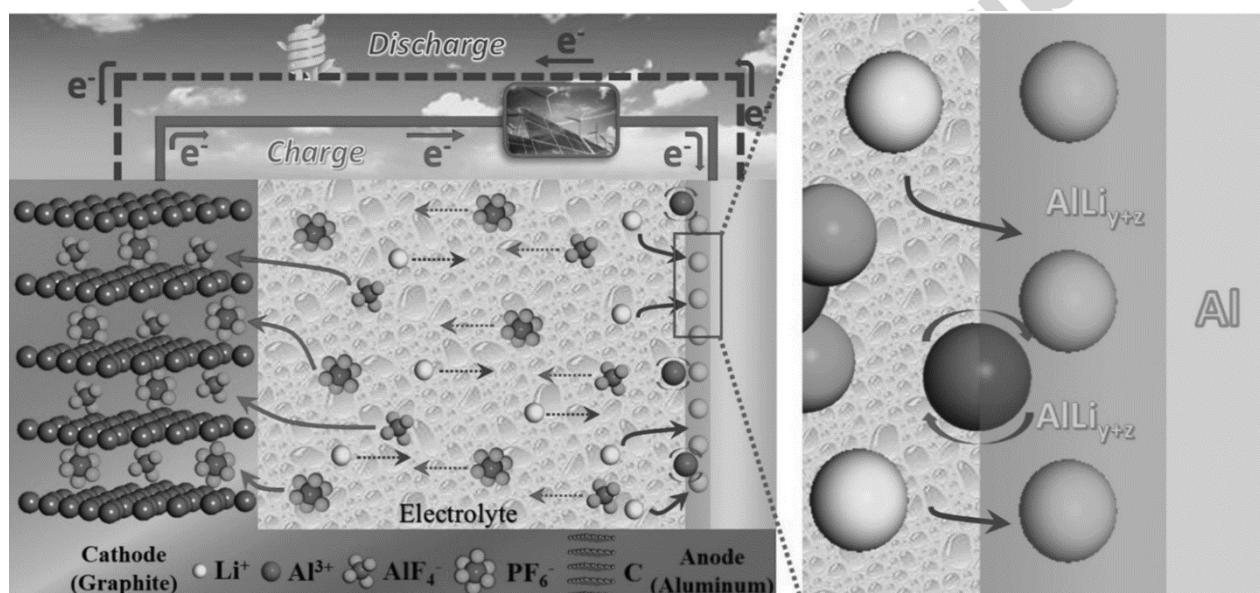


**Figure 15.** Schematic illustration of the multi-ions battery during the charging and discharging process. (+) Graphite/liquid electrolyte ( $\text{LiPF}_6 + \text{AlF}_3$  EMC-DMC, VC)/Celgard separator/Al foil (-) from left to right. On the cathode side, the complex anions ( $\text{PF}_6^-$  and  $\text{AlF}_4^-$ ) were intercalated/deintercalated into/from the graphite electrode during the charge/discharge process. On the anode side,  $\text{Li}^+$  was deposited on the surface of the Al foil and formed an  $\text{AlLi}_x$  alloy during the charge process, and then dissolved into the electrolyte again during discharge process. In the whole process,  $\text{AlF}_3$  first strengthened energy storage as well as protected the Al foil anode from dissolving [178]. Copyright (2017) John Wiley and Sons.



**Figure 16b,c** illustrates the graphite cathode and an assembled pouch cell; the voltage of the fully charged battery can reach to  $\sim 4.5$  V vs.  $\text{Li}^+/\text{AlLi}_x$ . The battery can light up a green light emitting diode (LED) lamp (**Figure 16d,e**), and the duration for lighting up of a LED lamp is over 96 hours. **Figure 16f** shows the charge/discharge curves of the battery at a charge current density of  $200 \text{ mA g}^{-1}$  and a discharge current density of  $100 \text{ mA g}^{-1}$  within the voltage range of 3.0–5.0 V vs.  $\text{Li}^+/\text{AlLi}_x$ . The charge curves displayed two voltage plateaus (stage 1: 4.2–4.4 V and stage 2: 4.5–4.7 V), and the charge capacity continuously dropped in the first three cycles due to the formation of SEI [32]. During the discharge process, two voltage plateaus at 4.2–4.4 V (stage 3) and 3.8–4.0 V (stage 4) were also observed, corresponding to the de-intercalation process. A capacity of  $\sim 120 \text{ mA h g}^{-1}$ , and no discharge capacity decay were observed in the subsequent cycles. Additionally, the battery can be also charged/discharged over 300 cycles, and the corresponding results are shown in **Figure 16g**. After 300 cycles, the battery delivered a reversible discharge capacity of  $\sim 113 \text{ mAh g}^{-1}$ , which was equivalent to 94.2% of the initial capacity, while the CE increased from 75% at the 10th cycle to nearly 95% in the subsequent cycles.

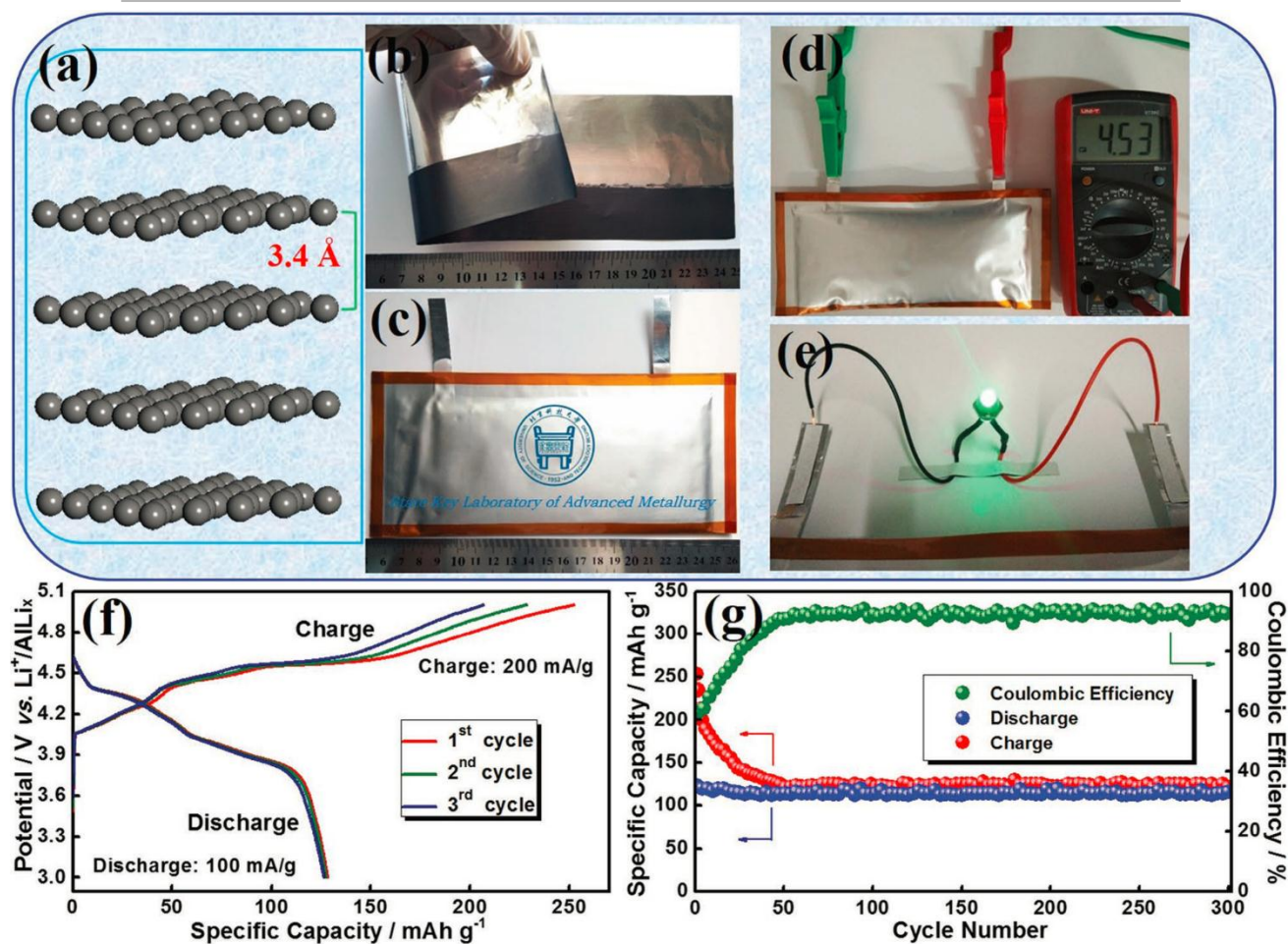


**Figure 16.** a) Schematic representation of the graphite crystal structure; the layer spacing is  $\approx 0.34\text{nm}$  b,c) The prepared graphite cathode and the assembled pouch cell. d,e) The voltage measurement of the fully charged battery and the battery lighting up a green LED lamp. f) The initial three charge–discharge curves of the battery in the potential range of 3.0-5.0 V versus  $\text{Li}^+/\text{AlLi}_x$ . g) The cycling performance and CE of over 300 cycles at a charge and discharge current density of 200 and 100 mA  $\text{g}^{-1}$ , respectively [178]. Copyright (2017) John Wiley and Sons.

**Table 2.** DIB systems and electrical performance of reported results.

Ref	Cathode	Anode	Electrolyte	Voltage region	Specific capacity	Cycling capability
[179]	KS-6 Graphite	$\text{MnO}_3$	$\text{LiPF}_6$	1.5-3.5	81 $\text{mAh g}^{-1}$	200 (90% from 3rd to 2nd)
[130]	Graphite	RGO	$\text{EMIm PF}_6$	0-4	30.3 $\text{F g}^{-1}$	74% after 50 cycles at 1.33 $\text{A g}^{-1}$
[158]	Graphite	Al foil	4 M $\text{LiPF}_6/\text{EMC}$ with 2 wt% VC	3-4.95	105 $\text{mAh g}^{-1}$ at 50 mA $\text{g}^{-1}$ 100 $\text{mAh g}^{-1}$ at 200 mA $\text{g}^{-1}$	88% after 200 cycles at 200 mA/g

[159]	MCMB	Al	1 M LiTFSI in Pyr <sub>14</sub> TFSI and 10% FEC	3-4.8	100, 97, 94, 92, and 85 mAh g <sup>-1</sup> at 0.5, 1, 2, 3, and 5 C	≈98 mAh g <sup>-1</sup> after 300 cycles at 0.5 C
[160]	Graphite	Porous Al/C	4 M LiPF <sub>6</sub> /EMC with 5 wt% VC	3.0–4.95	104, 103, 102, 95, and 85 mAh g <sup>-1</sup> at 2, 5, 10, 15, and 20 C	89.4% after 1000 cycles
[161]	Graphite	Bubble-She et-Like Interface Al anode	4 M LiPF <sub>6</sub> /EMC	3.0–4.95	106, 104, 103, 100, 98, and 85 mAh g <sup>-1</sup> at 1, 2, 3, 4, 5, and 10 C	99 % after 1500 cycles
[131]	Graphite	Graphite	Pyr <sub>14</sub> TFSI	1-5 V(disch arge plateau 4.4V)	82.0, 73.0, 47.7, and 24.0 mAh g <sup>-1</sup> at a rate of 0.3, 0.8, 2, and 4C	100% after 600 cycles
[129]	Graphite	Soft Carbon	1 M NaPF <sub>6</sub> in EC/DMC, 6:4, v/v	discharg e plateau 3.58 V, 2 - 4.5 V	100, 73, 56, 47, and 40 mAh g <sup>-1</sup> at 200, 500, 1000, 1500, and 2000 mA g <sup>-1</sup>	81.8% after 800 cycles
[180]	PTPAn	Graphite	0.8 M KPF <sub>6</sub> in EC:DEC (1:1, v/v)	3.23	44, 39, 35, 31, and 28 mAh g <sup>-1</sup> at 100, 150, 200, 250, and 300 mA g <sup>-1</sup>	75.5% after 500 cycles
[111]	Graphite	Nb <sub>2</sub> O <sub>5</sub>	1 M LiPF <sub>6</sub> /EC/D MC (1:2)	1.5-3.5	57 and 26 mAh g <sup>-1</sup> at 1C and 35C	Not reported
[81]	MCMB	CGP	1.7M LiPF <sub>6</sub> FEC–EMC (4 : 6 w/w) + 5mMHFIP,	1.5-5 V	Not reported	Not reported
[181]	polycyclic aromatic hydrocarbon	Li	LiPF <sub>6</sub> (1.0 M) in (EC)/ (DEC) (v/v 1:1)	2.5-4.2	39.9 mAh g <sup>-1</sup> ~21 mAh g <sup>-1</sup> at 500 mA g <sup>-1</sup>	after 960 cycles, 92%
[82]	KS6L graphite	CG graphite	Pyr <sub>14</sub> TFSI-1 M LiTFSI + 2% ES	3 - 5.1V	88 mAh g <sup>-1</sup>	~100% after 500 cycles 50 mAh g <sup>-1</sup> at 5C
[164]	graphite	Sn	1 M NaPF <sub>6</sub>	2.0–4.8	78, 74, 67, 65, and 61	94% after 400 cycles.

			in	V	mAh g <sup>-1</sup> at 1, 2, 3, 4,	
			EC+DMC+		and 5 C,	
			EMC (1:1:1			
			v/v/v)			
[109]	graphite	TiO <sub>2</sub>	1M LiPF <sub>6</sub> -EC:D MC (1:2 v/v)	3.7–1.5 V	Not reported	88.6% after 50 cycles
[178]	graphite	Al	LiPF <sub>6</sub> +AlF <sub>3</sub> EMC-DMC	3.0–5.0 V	≈120 mAh g <sup>-1</sup> at 100 mA g <sup>-1</sup>	~98% after 600 cycles,
[165]	expanded graphite	MCMB	1 M KPF <sub>6</sub> in EC-DMC-E MC (4:3:2 v/v/v)	3.0–5.2 V	61, 59, and 52 mAh g <sup>-1</sup> at 1, 2, and 3 C	82 mAh g <sup>-1</sup> at 1st cycle, and 61 mAh g <sup>-1</sup> at 100th cycles
[162]	graphite	Deposited Al	4 M LiPF <sub>6</sub> /EMC with 4 wt% VC	2.00–4.9 5 V	117.3, 116.8, and 116.1 mA h g <sup>-1</sup> at 60, 90, and 120 C,	≈61% at 60 C after 1500 cycles
[166]	expanded graphite	Sn	1 M KPF <sub>6</sub> in EC:DMC:E MC(4:3:2 v/v/v)	3.0–5.0 V,	50, 100, 200, and 300 mA g <sup>-1</sup> at 67, 63, 57, and 52 mAh g <sup>-1</sup>	93% for 300 cycles.
[163]	Graphite Nanoflakes	active carbon	Py <sub>14</sub> TFSI	2.25-5.2 5 V	70, and 61 mA g <sup>-1</sup> at 500, and 10000 mAh g <sup>-1</sup>	≈100 % after 200 cycles
[167]	3D graphene foam	Al	Al(ClO <sub>4</sub> ) <sub>3</sub> /P C-FEC	0.5-2 V (1 V)	101 mA h g <sup>-1</sup> at 2000 mA g <sup>-1</sup>	≈100 % after 150 cycles

EMC: ethyl-methyl carbonate; FEC: fluoroethylene carbonate; VC: vinylene carbonate; EC: ethylene carbonate ; DMC: dimethyl carbonate; DEC: diethyl carbonate; PC: propylene carbonate.

## 5. Conclusion and perspective

The application of graphite as cathode in rechargeable batteries, particularly in DIBs and AIBs, gained significant attention during the last few years. This perspective outlined the study of structure, mechanism of anion intercalated compound. Then, recent advance in various graphite cathode for the application in AIBs and DIBs are discussed. The discussion in this review has illustrated that significant amount of researches are devoted into enriching the anion intercalation devices. DIBs and

AIBs using graphitic materials as cathodes are promising energy storage devices ascribed to their relatively high energy density and low cost. Although considerable progress have been achieved, future research is still necessary to deal with the following challenges:

(1) Relatively lower CE. DIBs and AIBs deliver a low CE especially under lower rate and at the beginning several cycles. This is partly because the intercalation voltage is out of the stable voltage window of electrolyte from cathode, and partially resulted from the unstable SEI formed at the anode when using high specific capacity and low reaction potential alloying type anode, i.e. Al, Sn *etc.* The low CE from the anode should be solved flowing LIB solutions through electrode modification (nano sizing or nano composition) and electrolyte additive (get stable SEI). However, the modification of the graphitic cathode and the exploration of suitable electrolyte is a tremendous task, which requires deep thought and painstaking exploration.

(2) The specific capacity of the cathode materials are relatively low, less than  $124 \text{ mAh g}^{-1}$ , which is hard to satisfy the energy density required. Further increase of the cathode specific capacity is an oncoming task.

(3) Other aspects: The electrolyte dependence nature of DIBs indicates electrolyte with higher salt concentration is more appealing. In addition, the ratio of anode and cathode materials, as an important parameter, should be given more attention in future research and practical manufacture. Furthermore, current theoretical studies of anion intercalation behavior of graphite are mostly based on DFT, but the employment of MD, which should give powerful support of interfacial effect between the electrolyte and graphite, into anion intercalation system is highly demanded.

The probably strategies are:

(1) Possible strategies for higher CE: Read and Xu *et al.* [81] had developed high voltage

electrolyte based on a fluorinated solvent and additive, and proved the relatively better efficiency of the battery. The possible reasons should be: firstly, electrolyte solvents with the high working voltage would decrease side reactions of solvents at high voltage and thus increase CE at high voltage; secondly, electrolyte with high concentration can lower the intercalation potential and thus resulting in an acceptable electrochemical performance. In another aspect, Dai group had promoted the CE through adding an effective electrolyte additive [117]. Thus, researches on electrolyte additive should be also an important direction.

(2) Possible approaches for higher specific capacity are listed as follows:

(a) Firstly, anion intercalation graphite cathode is limited in space to store anion during charging process, thus searching for suitable multi-valent anion should be one of the possible solution to promote specific capacity.

(b) Secondly, two-dimensional molybdenum carbide (the chemical formula of molybdenum carbide is  $\text{Mo}_{1.33}\text{C}$ ) had shown the ability of anion intercalation [182], thus the development of other layered materials other than graphite would be a solution.

(c) Anion reaction mechanism rather than anion intercalation mechanism is reported with stable cycling performance [180]. And some positive charge-accepting cathode could give a higher specific capacity, such as tetrathiafulvalene derivative ( $196 \text{ mAh g}^{-1}$ ), antiaromatic porphyrinoid ( $200 \text{ mAh g}^{-1}$ ) and main-chain benzidine polymer ( $165 \text{ mAh g}^{-1}$ ) [183]. Thus, the development of novel anion reaction cathode materials with higher specific capacity and lower reaction voltage should be a viable solution. The use of positively charge-accepting cathode does have advantages: firstly, these cathode operate at moderate voltage in the stable operation window of solvents; secondly, the replacement of anion reaction mechanism from anion intercalation mechanism is potentially

exhibiting high specific capacity and thus high energy density.

## Acknowledgements

The authors gratefully acknowledge the financial support from the National Natural Science Foundation of China (Grant Nos. 51602337, 51702350), Shenzhen Peacock Plan (KQTD2016112915051055, KQJSCX20170331161244761), Natural Science Foundation of Guangdong Province (No. 2017A030310482), Shenzhen Science and Technology Planning Project (JCYJ20160122143155757, JSGG20160301173854530, JSGG20160301155933051, JSGG20160229202951528, JCYJ20170307171232348, JCYJ20170307172850024, JSGG20170413153302942), Guangdong Engineering Technology Research Center Foundation (No. 20151487), Shenzhen Engineering Laboratory Foundation (No. 20151837), and Scientific Project of Chinese Academy of Sciences (GJHS20170314161200165, KFJ-STS-SCYD-124).

## Reference

- [1] B. Dunn, H. Kamath, J.M. Tarascon, Electrical energy storage for the grid: A battery of choices, *Science* 334(6058) (2011) 928-935.
- [2] P. Simon, Y. Gogotsi, B. Dunn, Where do batteries end and supercapacitors begin?, *Science* 343(6176) (2014) 1210-1211.
- [3] M. Armand, J.M. Tarascon, Building better batteries, *Nature* 451(7179) (2008) 652-657.
- [4] J.B. Goodenough, Y. Kim, Challenges for rechargeable Li batteries, *Chem. Mater.* 22(3) (2010) 587-603.

- [5] C.M. Park, J.H. Kim, H. Kim, H.J. Sohn, Li-alloy based anode materials for Li secondary batteries, *Chem. Soc. Rev.* 39(8) (2010) 3115-3141.
- [6] B. Kang, G. Ceder, Battery materials for ultrafast charging and discharging, *Nature* 458(7235) (2009) 190-193.
- [7] X. Ji, K.T. Lee, L.F. Nazar, A highly ordered nanostructured carbon-sulphur cathode for lithium-sulphur batteries, *Nat. Mater.* 8(6) (2009) 500-506.
- [8] P.G. Bruce, B. Scrosati, J.M. Tarascon, Nanomaterials for rechargeable lithium batteries, *Angew. Chem. Int. Ed.* 47(16) (2008) 2930-2946.
- [9] H. Wang, H. Dai, Strongly coupled inorganic-nano-carbon hybrid materials for energy storage, *Chem. Soc. Rev.* 42(7) (2013) 3088-3113.
- [10] J.M. Tarascon, M. Armand, Issues and challenges facing rechargeable lithium batteries, *Nature* 414(6861) (2001) 359-367.
- [11] E. Yoo, J. Kim, E. Hosono, H. Zhou, T. Kudo, I. Honma, Large reversible Li storage of graphene nanosheet families for use in rechargeable lithium ion batteries, *Nano Lett.* 8(8) (2008) 2277-2282.
- [12] P. Simon, Y. Gogotsi, Materials for electrochemical capacitors, *Nat. Mater.* 7(11) (2008) 845-854.
- [13] P. Poizot, S. Laruelle, S. Grugeon, L. Dupont, J.M. Tarascon, Nano-sized transition-metaloxides as negative-electrode materials for lithium-ion batteries, *Nature* 407(6803) (2000) 496-499.
- [14] S. Chu, Y. Cui, N. Liu, The path towards sustainable energy, *Nat. Mater.* 16(1) (2016) 16-22.
- [15] V.R. Stamenkovic, D. Strmcnik, P.P. Lopes, N.M. Markovic, Energy and fuels from electrochemical interfaces, *Nat. Mater.* 16(1) (2016) 57-69.



- [16] G. Chen, L. Yan, H. Luo, S. Guo, Nanoscale engineering of heterostructured anode materials for boosting lithium-ion storage, *Adv. Mater.* 28(35) (2016) 7580-7602.
- [17] K. Zhang, G.-H. Lee, M. Park, W. Li, Y.-M. Kang, Recent developments of the lithium metal anode for rechargeable non-aqueous batteries, *Adv. Energy Mater.* 6(20) (2016) 1600811.
- [18] M.N. Obrovac, V.L. Chevrier, Alloy negative electrodes for Li-ion batteries, *Chem. Rev.* 114(23) (2014) 11444-11502.
- [19] M.S. Whittingham, Lithium batteries and cathode materials, *Chem. Rev.* 104(10) (2004) 4271-4301.
- [20] F. Bonaccorso, L. Colombo, G. Yu, M. Stoller, V. Tozzini, A.C. Ferrari, R.S. Ruoff, V. Pellegrini, Graphene, related two-dimensional crystals, and hybrid systems for energy conversion and storage, *Science* 347(6217) (2015) 1246501-1246503.
- [21] J.B. Goodenough, Evolution of strategies for modern rechargeable batteries, *Acc. Chem. Res.* 46(5) (2013) 1053-1061.
- [22] C. Liu, F. Li, L.P. Ma, H.M. Cheng, Advanced materials for energy storage, *Adv. Mater.* 22(8) (2010) E28-E62.
- [23] Y.-Z. Liu, Y.-F. Li, F.-Y. Su, L.-J. Xie, Q.-Q. Kong, X.-M. Li, J.-G. Gao, C.-M. Chen, Easy one-step synthesis of N-doped graphene for supercapacitors, *Energy Storage Mater.* 2 (2016) 69-75.
- [24] W. Lv, Z. Li, Y. Deng, Q.-H. Yang, F. Kang, Graphene-based materials for electrochemical energy storage devices: Opportunities and challenges, *Energy Storage Mater.* 2 (2016) 107-138.
- [25] J. Niu, R. Shao, M. Liu, J. Liang, Z. Zhang, M. Dou, Y. Huang, F. Wang, Porous carbon electrodes with battery-capacitive storage features for high performance Li-ion capacitors, *Energy Storage Mater.* 12 (2018) 145-152.

- [26] X. Shen, H. Liu, X.-B. Cheng, C. Yan, J.-Q. Huang, Beyond lithium ion batteries: higher energy density battery systems based on lithium metal anodes, *Energy Storage Mater.* 12 (2018) 161-175.
- [27] H. Wu, Y. Zhang, L. Cheng, L. Zheng, Y. Li, W. Yuan, X. Yuan, Graphene based architectures for electrochemical capacitors, *Energy Storage Mater.* 5 (2016) 8-32.
- [28] Z. Wu, J. Xu, Q. Zhang, H. Wang, S. Ye, Y. Wang, C. Lai, LiI embedded meso-micro porous carbon polyhedrons for lithium iodine battery with superior lithium storage properties, *Energy Storage Mater.* 10 (2018) 62-68.
- [29] L. Yue, J. Ma, J. Zhang, J. Zhao, S. Dong, Z. Liu, G. Cui, L. Chen, All solid-state polymer electrolytes for high-performance lithium ion batteries, *Energy Storage Mater.* 5 (2016) 139-164.
- [30] B. Zhao, D. Chen, X. Xiong, B. Song, R. Hu, Q. Zhang, B.H. Rainwater, G.H. Waller, D. Zhen, Y. Ding, Y. Chen, C. Qu, D. Dang, C.-P. Wong, M. Liu, A high-energy, long cycle-life hybrid supercapacitor based on graphene composite electrodes, *Energy Storage Mater.* 7 (2017) 32-39.
- [31] Y. Zhao, Z. Song, X. Li, Q. Sun, N. Cheng, S. Lawes, X. Sun, Metal organic frameworks for energy storage and conversion, *Energy Storage Mater.* 2 (2016) 35-62.
- [32] A. Eftekhari, Low voltage anode materials for lithium-ion batteries, *Energy Storage Mater.* 7 (2017) 157-180.
- [33] Y. Li, M.-Q. Wang, Y. Chen, L. Hu, T. Liu, S. Bao, M. Xu, Muscle-like electrode design for Li-Te batteries, *Energy Storage Mater.* 10 (2018) 10-15.
- [34] Y. Liu, Y. Qiao, Y. Zhang, Z. Yang, T. Gao, D. Kirsch, B. Liu, J. Song, B. Yang, L. Hu, 3D printed separator for the thermal management of high-performance Li metal anodes, *Energy Storage Mater.* 12 (2018) 197-203.
- [35] J. Cui, S. Yao, J.-K. Kim, Recent progress in rational design of anode materials for

- high-performance Na-ion batteries, *Energy Storage Mater.* 7 (2017) 64-114.
- [36] S. Dong, Y. Xu, L. Wu, H. Dou, X. Zhang, Surface-functionalized graphene-based quasi-solid-state Na-ion hybrid capacitors with excellent performance, *Energy Storage Mater.* 11 (2018) 8-15.
- [37] Z. Ju, P. Li, G. Ma, Z. Xing, Q. Zhuang, Y. Qian, Few layer nitrogen-doped graphene with highly reversible potassium storage, *Energy Storage Mater.* 11 (2018) 38-46.
- [38] W. Li, X. Guo, Y. Lu, L. Wang, A. Fan, M. Sui, H. Yu, Amorphous nanosized silicon with hierarchically porous structure for high-performance lithium ion batteries, *Energy Storage Mater.* 7 (2017) 203-208.
- [39] Z. Lu, Z. Zhang, X. Chen, Q. Chen, F. Ren, M. Wang, S. Wu, Z. Peng, D. Wang, J. Ye, Improving Li anode performance by a porous 3D carbon paper host with plasma assisted sponge carbon coating, *Energy Storage Mater.* 11 (2018) 47-56.
- [40] Y. Wang, R. Chen, T. Chen, H. Lv, G. Zhu, L. Ma, C. Wang, Z. Jin, J. Liu, Emerging non-lithium ion batteries, *Energy Storage Mater.* 4 (2016) 103-129.
- [41] M.R. Palacin, Recent advances in rechargeable battery materials: a chemist's perspective, *Chem. Soc. Rev.* 38(9) (2009) 2565-2575.
- [42] S. Hy, H. Liu, M. Zhang, D. Qian, B.-J. Hwang, Y.S. Meng, Performance and design considerations for lithium excess layered oxide positive electrode materials for lithium ion batteries, *Energy Environ. Sci* 9(6) (2016) 1931-1954.
- [43] M. Noel, R. Santhanam, Electrochemistry of graphite intercalation compounds, *J. Power Sources* 72(1) (1998) 53-65.
- [44] J.A. Seel, J.R. Dahn, Electrochemical intercalation of PF 6 into graphite, *J. Electrochem. Soc.*

147(3) (2000) 892-898.

[45] D.A. Dikin, S. Stankovich, E.J. Zimney, R.D. Piner, G.H.B. Dommett, G. Evmenenko, S.T. Nguyen, R.S. Ruoff, Preparation and characterization of graphene oxide paper, *Nature* 448(7152) (2007) 457-460.

[46] C. Kim, B.T.N. Ngoc, K.S. Yang, M. Kojima, Y.A. Kim, Y.J. Kim, M. Endo, S.C. Yang, Self-sustained thin webs consisting of porous carbon nanofibers for supercapacitors via the electrospinning of polyacrylonitrile solutions containing zinc chloride, *Adv. Mater.* 19(17) (2007) 2341-2346.

[47] W.C. West, J.F. Whitacre, N. Leifer, S. Greenbaum, M. Smart, R. Bugga, M. Blanco, S.R. Narayanan, Reversible intercalation of fluoride-anion receptor complexes in graphite, *J. Electrochem. Soc.* 154(10) (2007) A929-A936.

[48] R.-G. Xiao, K.-P. Yan, J.-X. Yan, J.-Z. Wang, Electrochemical etching model in aluminum foil for capacitor, *Corros. Sci.* 50(6) (2008) 1576-1583.

[49] Z.S. Wu, Y. Zheng, S. Zheng, S. Wang, C. Sun, K. Parvez, T. Ikeda, X. Bao, K. Müllen, X. Feng, Stacked - Layer Heterostructure Films of 2D Thiophene Nanosheets and Graphene for High - Rate All - Solid - State Pseudocapacitors with Enhanced Volumetric Capacitance, *Adv. Mater.* 29(3) (2017) 1602960.

[50] Z.S. Wu, K. Parvez, S. Li, S. Yang, Z. Liu, S. Liu, X. Feng, K. Müllen, Alternating Stacked Graphene - Conducting Polymer Compact Films with Ultrahigh Areal and Volumetric Capacitances for High - Energy Micro - Supercapacitors, *Adv. Mater.* 27(27) (2015) 4054-4061.

[51] I.A. Rodriguez-Perez, X. Ji, Anion hosting cathodes in dual-ion batteries, *ACS Energy Lett.* 2(8) (2017) 1762-1770.

- [52] G.A. Elia, K. Marquardt, K. Hoepfner, S. Fantini, R. Lin, E. Knipping, W. Peters, J.F. Drillet, S. Passerini, R. Hahn, An overview and future perspectives of aluminum batteries, *Adv. Mater.* 28(35) (2016) 7564-7579.
- [53] M.V. Reddy, G.V. Subba Rao, B.V. Chowdari, Metal oxides and oxysalts as anode materials for Li ion batteries, *Chem. Rev.* 113(7) (2013) 5364-5457.
- [54] M. Zhang, T. Zhang, Y. Ma, Y. Chen, Latest development of nanostructured Si/C materials for lithium anode studies and applications, *Energy Storage Mater.* 4 (2016) 1-14.
- [55] Q.C. Liu, J.J. Xu, S. Yuan, Z.W. Chang, D. Xu, Y.B. Yin, L. Li, H.X. Zhong, Y.S. Jiang, J.M. Yan, X.B. Zhang, Artificial protection film on lithium metal anode toward long-cycle-life lithium-oxygen batteries, *Adv. Mater.* 27(35) (2015) 5241-5247.
- [56] J. Qian, W.A. Henderson, W. Xu, P. Bhattacharya, M. Engelhard, O. Borodin, J.G. Zhang, High rate and stable cycling of lithium metal anode, *Nat. Commun.* 6 (2015) 6362.
- [57] C.P. Yang, Y.X. Yin, S.F. Zhang, N.W. Li, Y.G. Guo, Accommodating lithium into 3D current collectors with a submicron skeleton towards long-life lithium metal anodes, *Nat. Commun.* 6 (2015) 8058.
- [58] X.B. Cheng, T.Z. Hou, R. Zhang, H.J. Peng, C.Z. Zhao, J.Q. Huang, Q. Zhang, Dendrite-free lithium deposition induced by uniformly distributed lithium ions for efficient lithium metal batteries, *Adv. Mater.* 28(15) (2016) 2888-2895.
- [59] S. Jin, S. Xin, L. Wang, Z. Du, L. Cao, J. Chen, X. Kong, M. Gong, J. Lu, Y. Zhu, H. Ji, R.S. Ruoff, Covalently connected carbon nanostructures for current collectors in both the cathode and anode of Li-S batteries, *Adv. Mater.* 28(41) (2016) 9094-9102.
- [60] N.W. Li, Y.X. Yin, C.P. Yang, Y.G. Guo, An artificial solid electrolyte interphase layer for

stable lithium metal anodes, *Adv. Mater.* 28(9) (2016) 1853-1858.

[61] D. Lin, Y. Liu, Z. Liang, H.W. Lee, J. Sun, H. Wang, K. Yan, J. Xie, Y. Cui, Layered reduced graphene oxide with nanoscale interlayer gaps as a stable host for lithium metal anodes, *Nat. Nanotechnol.* 11(7) (2016) 626-632.

[62] L.L. Lu, J. Ge, J.N. Yang, S.M. Chen, H.B. Yao, F. Zhou, S.H. Yu, Free-standing copper nanowire network current collector for improving lithium anode performance, *Nano Lett.* 16(7) (2016) 4431-4437.

[63] S. Wenzel, S. Randau, T. Leichtweiß, D.A. Weber, J. Sann, W.G. Zeier, J. Janek, Direct observation of the interfacial instability of the fast ionic conductor  $\text{Li}_{10}\text{GeP}_2\text{S}_{12}$  at the lithium metal anode, *Chem. Mater.* 28(7) (2016) 2400-2407.

[64] K. Yan, Z. Lu, H.-W. Lee, F. Xiong, P.-C. Hsu, Y. Li, J. Zhao, S. Chu, Y. Cui, Selective deposition and stable encapsulation of lithium through heterogeneous seeded growth, *Nat. Energy* 1(3) (2016) 16010.

[65] Y. Liu, D. Lin, P.Y. Yuen, K. Liu, J. Xie, R.H. Dauskardt, Y. Cui, An artificial solid electrolyte interphase with high Li-ion conductivity, mechanical strength, and flexibility for stable lithium metal anodes, *Adv. Mater.* 29(10) (2017) 1605531.

[66] J. Zhao, G. Zhou, K. Yan, J. Xie, Y. Li, L. Liao, Y. Jin, K. Liu, P.-C. Hsu, J. Wang, H.-M. Cheng, Y. Cui, Air-stable and freestanding lithium alloy/graphene foil as an alternative to lithium metal anodes, *Nat. Nanotechnol.* 12 (2017) 993-999.

[67] J. Wang, X. He, E. Paillard, N. Laszczynski, J. Li, S. Passerini, Lithium- and manganese-rich oxide cathode materials for high-energy lithium ion batteries, *Adv. Energy Mater.* 6(21) (2016) 1600906.

- [68] S. Dou, Review and prospect of layered lithium nickel manganese oxide as cathode materials for Li-ion batteries, *J. Solid State Electrochem.* 17(4) (2013) 911-926.
- [69] J. Lu, Z. Chen, Z. Ma, F. Pan, L.A. Curtiss, K. Amine, The role of nanotechnology in the development of battery materials for electric vehicles, *Nat. Nanotechnol.* 11(12) (2016) 1031-1038.
- [70] J. Hong, H. Gwon, S.-K. Jung, K. Ku, K. Kang, Review—lithium-excess layered cathodes for lithium rechargeable batteries, *J. Electrochem. Soc.* 162(14) (2015) A2447-A2467.
- [71] Z.-S. Wu, Y.-Z. Tan, S. Zheng, S. Wang, K. Parvez, J. Qin, X. Shi, C. Sun, X. Bao, X. Feng, K. Müllen, Bottom-Up Fabrication of Sulfur-Doped Graphene Films Derived from Sulfur-Annulated Nanographene for Ultrahigh Volumetric Capacitance Micro-Supercapacitors, *J. Am. Chem. Soc.* 139(12) (2017) 4506-4512.
- [72] R. Fang, S. Zhao, Z. Sun, D.W. Wang, H.M. Cheng, F. Li, More Reliable Lithium - Sulfur Batteries: Status, Solutions and Prospects, *Adv. Mater.* 29(48) (2017) 1606823.
- [73] L. Ji, P. Meduri, V. Agubra, X. Xiao, M. Alcoutlabi, Graphene-based nanocomposites for energy storage, *Adv. Energy Mater.* 6(16) (2016) 1502159.
- [74] A. Ambrosi, C.K. Chua, A. Bonanni, M. Pumera, Electrochemistry of graphene and related materials, *Chem. Rev.* 114(14) (2014) 7150-7188.
- [75] M.R. Lukatskaya, B. Dunn, Y. Gogotsi, Multidimensional materials and device architectures for future hybrid energy storage, *Nat. Commun.* 7 (2016) 12647.
- [76] Y. Ma, H. Chang, M. Zhang, Y. Chen, Graphene-based materials for lithium-ion hybrid supercapacitors, *Adv. Mater.* 27(36) (2015) 5296-5308.
- [77] S. Zheng, Z.-S. Wu, S. Wang, H. Xiao, F. Zhou, C. Sun, X. Bao, H.-M. Cheng, Graphene-based materials for high-voltage and high-energy asymmetric supercapacitors, *Energy Storage Mater.* 6

(2017) 70-97.

[78] T. Deng, W. Zhang, O. Arcelus, J.-G. Kim, J. Carrasco, S.J. Yoo, W. Zheng, J. Wang, H. Tian, H. Zhang, X. Cui, T. Rojo, Atomic-level energy storage mechanism of cobalt hydroxide electrode for pseudocapacitors, *Nat. Commun.* 8 (2017) 15194.

[79] L. Zhang, F. Zhang, X. Yang, G. Long, Y. Wu, T. Zhang, K. Leng, Y. Huang, Y. Ma, A. Yu, Y. Chen, Porous 3D graphene-based bulk materials with exceptional high surface area and excellent conductivity for supercapacitors, *Sci. Rep.* 3 (2013) 1408.

[80] M. Zhang, Z. Sun, T. Zhang, B. Qin, D. Sui, Y. Xie, Y. Ma, Y. Chen, Porous asphalt/graphene composite for supercapacitors with high energy density at superior power density without added conducting materials, *J. Mater. Chem. A* 5(41) (2017) 21757-21764.

[81] J.A. Read, A.V. Cresce, M.H. Ervin, K. Xu, Dual-graphite chemistry enabled by a high voltage electrolyte, *Energy Environ. Sci* 7(2) (2014) 617-620.

[82] S. Rothermel, P. Meister, G. Schmuelling, O. Fromm, H.-W. Meyer, S. Nowak, M. Winter, T. Placke, Dual-graphite cells based on the reversible intercalation of bis(trifluoromethanesulfonyl)imide anions from an ionic liquid electrolyte, *Energy Environ. Sci* 7(10) (2014) 3412-3423.

[83] S. Wang, Z. Yu, J. Tu, J. Wang, D. Tian, Y. Liu, S. Jiao, A novel aluminum-ion battery: Al/AlCl<sub>3</sub>-[EMIm]Cl/Ni<sub>3</sub>S<sub>2</sub>@graphene, *Adv. Energy Mater.* 6(13) (2016) 1600137.

[84] T. Gao, X. Li, X. Wang, J. Hu, F. Han, X. Fan, L. Suo, A.J. Pearse, S.B. Lee, G.W. Rubloff, K.J. Gaskell, M. Noked, C. Wang, A rechargeable Al/S battery with an ionic-liquid electrolyte, *Angew. Chem. Int. Ed.* 55(34) (2016) 9898-9901.

[85] P. Bhauriyal, A. Mahata, B. Pathak, The staging mechanism of AlCl<sub>4</sub> intercalation in a graphite



- electrode for an aluminium-ion battery, *Phys. Chem. Chem. Phys.* 19(11) (2017) 7980-7989.
- [86] Y. Li, Y. Lu, C. Zhao, Y.-S. Hu, M.-M. Titirici, H. Li, X. Huang, L. Chen, Recent advances of electrode materials for low-cost sodium-ion batteries towards practical application for grid energy storage, *Energy Storage Mater.* 7 (2017) 130-151.
- [87] Y. Li, L. Mu, Y.-S. Hu, H. Li, L. Chen, X. Huang, Pitch-derived amorphous carbon as high performance anode for sodium-ion batteries, *Energy Storage Mater.* 2 (2016) 139-145.
- [88] K. Kubota, S. Komaba, Review—practical issues and future perspective for Na-ion batteries, *J. Electrochem. Soc.* 162(14) (2015) A2538-A2550.
- [89] D. Gong, B. Wang, J. Zhu, R. Podila, A.M. Rao, X. Yu, Z. Xu, B. Lu, An iodine quantum dots based rechargeable sodium–iodine battery, *Adv. Energy Mater.* 7(3) (2017) 1601885.
- [90] C. Lee, S.-K. Jeong, A novel superconcentrated aqueous electrolyte to improve the electrochemical performance of calcium-ion batteries, *Chem. Lett.* 45(12) (2016) 1447-1449.
- [91] M. Cabello, F. Nacimiento, J.R. González, G. Ortiz, R. Alcántara, P. Lavela, C. Pérez-Vicente, J.L. Tirado, Advancing towards a veritable calcium-ion battery:  $\text{CaCo}_2\text{O}_4$  positive electrode material, *Electrochem. Commun.* 67 (2016) 59-64.
- [92] R.Y. Wang, C.D. Wessells, R.A. Huggins, Y. Cui, Highly reversible open framework nanoscale electrodes for divalent ion batteries, *Nano Lett.* 13(11) (2013) 5748-5752.
- [93] A. Ponrouch, C. Frontera, F. Barde, M.R. Palacin, Towards a calcium-based rechargeable battery, *Nat. Mater.* 15(2) (2016) 169-172.
- [94] D. Aurbach, Z. Lu, A. Schechter, Y. Gofer, H. Gizbar, R. Turgeman, Y. Cohen, M. Moshkovich, E. Levi, Prototype systems for rechargeable magnesium batteries, *Nature* 407 (2000) 724-727.

- [95] D. Er, E. Detsi, H. Kumar, V.B. Shenoy, Defective graphene and graphene allotropes as high-capacity anode materials for Mg ion batteries, *ACS Energy Lett.* 1(3) (2016) 638-645.
- [96] G. Xin, X. Wang, C. Wang, J. Zheng, X. Li, Porous Mg thin films for Mg-air batteries, *Dalton Trans* 42(48) (2013) 16693-16696.
- [97] J. Wu, G. Gao, G. Wu, B. Liu, H. Yang, X. Zhou, J. Wang, MgVPO<sub>4</sub>F as a one-dimensional Mg-ion conductor for Mg ion battery positive electrode: a first principles calculation, *RSC Adv.* 4(29) (2014) 15014-15017.
- [98] F. Wang, F. Yu, X. Wang, Z. Chang, L. Fu, Y. Zhu, Z. Wen, Y. Wu, W. Huang, Aqueous rechargeable zinc/aluminum ion battery with good cycling performance, *ACS Appl Mater Interfaces* 8(14) (2016) 9022-9029.
- [99] M.L. Agiorgousis, Y.-Y. Sun, S. Zhang, The role of ionic liquid electrolyte in an aluminum-graphite electrochemical cell, *ACS Energy Lett.* 2(3) (2017) 689-693.
- [100] S. Liu, J.J. Hu, N.F. Yan, G.L. Pan, G.R. Li, X.P. Gao, Aluminum storage behavior of anatase TiO<sub>2</sub> nanotube arrays in aqueous solution for aluminum ion batteries, *Energy Environ. Sci* 5(12) (2012) 9743.
- [101] H. Yang, L. Yin, J. Liang, Z. Sun, Y. Wang, H. Li, K. He, L. Ma, Z. Peng, S. Qiu, C. Sun, H.M. Cheng, F. Li, An Aluminum–Sulfur Battery with a Fast Kinetic Response, *Angew. Chem. Int. Ed.* 57(7) (2018) 1898-1902.
- [102] Y. Xu, Y. Zhao, J. Ren, Y. Zhang, H. Peng, An all-solid-state fiber-shaped aluminum-air battery with flexibility, stretchability, and high electrochemical performance, *Angew. Chem. Int. Ed.* 55(28) (2016) 7979-7982.
- [103] E. Grishina, D. Gelman, S. Belopukhov, D. Starosvetsky, A. Groysman, Y. Ein-Eli,

Improvement of aluminum-air battery performances by the application of flax straw extract, *ChemSusChem* 9(16) (2016) 2103-2111.

[104] M.C. Lin, M. Gong, B. Lu, Y. Wu, D.Y. Wang, M. Guan, M. Angell, C. Chen, J. Yang, B.J. Hwang, H. Dai, An ultrafast rechargeable aluminium-ion battery, *Nature* 520(7547) (2015) 325-328.

[105] X. Yu, B. Wang, D. Gong, Z. Xu, B. Lu, Graphene nanoribbons on highly porous 3D graphene for high - capacity and ultrastable Al - ion batteries, *Adv. Mater.* 29(4) (2017) 1604118.

[106] Y. Fang, Y. Lv, R. Che, H. Wu, X. Zhang, D. Gu, G. Zheng, D. Zhao, Two-dimensional mesoporous carbon nanosheets and their derived graphene nanosheets: synthesis and efficient lithium ion storage, *J. Am. Chem. Soc.* 135(4) (2013) 1524-1530.

[107] R.T. Carlin, Dual intercalating molten electrolyte batteries, *J. Electrochem. Soc.* 141(7) (1994) L73-L76.

[108] T.E. Sutto, T.T. Duncan, T.C. Wong, X-ray diffraction studies of electrochemical graphite intercalation compounds of ionic liquids, *Electrochim. Acta* 54(24) (2009) 5648-5655.

[109] A.K. Thapa, G. Park, H. Nakamura, T. Ishihara, N. Moriyama, T. Kawamura, H. Wang, M. Yoshio, Novel graphite/TiO<sub>2</sub> electrochemical cells as a safe electric energy storage system, *Electrochim. Acta* 55(24) (2010) 7305-7309.

[110] H. Wang, M. Yoshio, Suppression of PF<sub>6</sub><sup>-</sup> intercalation into graphite by small amounts of ethylene carbonate in activated carbon/graphite capacitors, *Chem. Commun.* 46(9) (2010) 1544-1546.

[111] G. Park, N. Gunawardhana, C. Lee, S.-M. Lee, Y.-S. Lee, M. Yoshio, Development of a novel and safer energy storage system using a graphite cathode and Nb<sub>2</sub>O<sub>5</sub> anode, *J. Power Sources* 236 (2013) 145-150.

- [112] X. Yang, F. Zhang, L. Zhang, T.F. Zhang, Y. Huang, Y.S. Chen, A high-performance graphene oxide-doped ion gel as gel polymer electrolyte for all-solid-state supercapacitor applications, *Adv. Funct. Mater.* 23(26) (2013) 3353-3360.
- [113] Q. Chen, Y. Meng, C. Hu, Y. Zhao, H. Shao, N. Chen, L. Qu, MnO<sub>2</sub>-modified hierarchical graphene fiber electrochemical supercapacitor, *J. Power Sources* 247 (2014) 32-39.
- [114] P. Meister, V. Siozios, J. Reiter, S. Klamor, S. Rothermel, O. Fromm, H.-W. Meyer, M. Winter, T. Placke, Dual-ion cells based on the electrochemical intercalation of asymmetric fluorosulfonyl-(trifluoromethanesulfonyl) imide anions into graphite, *Electrochim. Acta* 130 (2014) 625-633.
- [115] H. Nakano, Y. Sugiyama, T. Morishita, M.J.S. Spencer, I.K. Snook, Y. Kumai, H. Okamoto, Anion secondary batteries utilizing a reversible BF<sub>4</sub> insertion/extraction two-dimensional Si material, *J. Mater. Chem. A* 2(20) (2014) 7588.
- [116] X. Qi, B. Blizanac, A. DuPasquier, P. Meister, T. Placke, M. Oljaca, J. Li, M. Winter, Investigation of PF<sub>6</sub>(-) and TFSI(-) anion intercalation into graphitized carbon blacks and its influence on high voltage lithium ion batteries, *Phys. Chem. Chem. Phys.* 16(46) (2014) 25306-25313.
- [117] M. Angell, C.-J. Pan, Y. Rong, C. Yuan, M.-C. Lin, B.-J. Hwang, H. Dai, High coulombic efficiency aluminum-ion battery using an AlCl<sub>3</sub>-urea ionic liquid analog electrolyte, *Proc. Natl. Acad. Sci. USA.* 114(5) (2017) 834-839.
- [118] D.Y. Wang, C.Y. Wei, M.C. Lin, C.J. Pan, H.L. Chou, H.A. Chen, M. Gong, Y. Wu, C. Yuan, M. Angell, Y.J. Hsieh, Y.H. Chen, C.Y. Wen, C.W. Chen, B.J. Hwang, C.C. Chen, H. Dai, Advanced rechargeable aluminium ion battery with a high-quality natural graphite cathode, *Nat.*

Commun. 8 (2017) 14283.

[119] K. Tasaki, Density functional theory study on structural and energetic characteristics of graphite intercalation compounds, *J. Phys. Chem. C* 118(3) (2014) 1443-1450.

[120] M.S. Wu, B. Xu, L.Q. Chen, C.Y. Ouyang, Geometry and fast diffusion of  $\text{AlCl}_4$  cluster intercalated in graphite, *Electrochim. Acta* 195 (2016) 158-165.

[121] S.C. Jung, Y.-J. Kang, D.-J. Yoo, J.W. Choi, Y.-K. Han, Flexible few-layered graphene for the ultrafast rechargeable aluminum-ion battery, *J. Phys. Chem. C* 120(25) (2016) 13384-13389.

[122] S. Grimme, Semiempirical GGA-type density functional constructed with a long-range dispersion correction, *J. Comput. Chem.* 27(15) (2006) 1787-1799.

[123] S. Grimme, J. Antony, S. Ehrlich, H. Krieg, A consistent and accurate ab initio parametrization of density functional dispersion correction (DFT-D) for the 94 elements H-Pu, *The Journal of Chemical Physics* 132(15) (2010) 154104.

[124] G. Mills, H. Jónsson, G.K. Schenter, Reversible work transition state theory: application to dissociative adsorption of hydrogen, *Surf. Sci.* 324(2) (1995) 305-337.

[125] E.M. Perassi, E.P.M. Leiva, A theoretical model to determine intercalation entropy and enthalpy: Application to lithium/graphite, *Electrochem. Commun.* 65 (2016) 48-52.

[126] S. Miyoshi, T. Akbay, T. Kurihara, T. Fukuda, A.T. Staykov, S. Ida, T. Ishihara, Fast diffusivity of  $\text{PF}_6^-$  anions in graphitic carbon for a dual-carbon rechargeable battery with superior rate property, *J. Phys. Chem. C* 120(40) (2016) 22887-22894.

[127] S. Zhang, M. Wang, Z. Zhou, Y. Tang, Multifunctional electrode design consisting of 3D porous separator modulated with patterned anode for high-performance dual-Ion batteries, *Adv. Funct. Mater.* 27(39) (2017) 1703035.

- [128] S.J. An, J. Li, C. Daniel, D. Mohanty, S. Nagpure, D.L. Wood, The state of understanding of the lithium-ion-battery graphite solid electrolyte interphase (SEI) and its relationship to formation cycling, *Carbon* 105 (2016) 52-76.
- [129] L. Fan, Q. Liu, S. Chen, Z. Xu, B. Lu, Soft carbon as anode for high-performance sodium-based dual ion full battery, *Adv. Energy Mater.* 7(14) (2017) 1602778.
- [130] X. Shi, W. Zhang, J. Wang, W. Zheng, K. Huang, H. Zhang, S. Feng, H. Chen, (EMIm)<sup>+</sup>(PF6)<sup>-</sup> ionic liquid unlocks optimum energy/power density for architecture of nanocarbon-based dual-ion battery, *Adv. Energy Mater.* 6(24) (2016) 1601378.
- [131] J. Fan, Z. Zhang, Y. Liu, A. Wang, L. Li, W. Yuan, An excellent rechargeable PP14TFSI ionic liquid dual-ion battery, *Chem. Commun.* 53(51) (2017) 6891-6894.
- [132] K. Beltrop, P. Meister, S. Klein, A. Heckmann, M. Grünebaum, H.-D. Wiemhöfer, M. Winter, T. Placke, Does size really matter? new insights into the intercalation behavior of anions into a graphite-based positive electrode for dual-ion batteries, *Electrochim. Acta* 209 (2016) 44-55.
- [133] P. Bieker, M. Winter, High energy accumulators lithium-ion-technology and what might come next, *Chem. unserer Zeit* 50(3) (2016) 172-186.
- [134] E. Deunf, P. Jimenez, D. Guyomard, F. Dolhem, P. Poizot, A dual-ion battery using diamino-rubicene as anion-inserting positive electrode material, *Electrochem. Commun.* 72 (2016) 64-68.
- [135] P. Meister, G. Schmuelling, M. Winter, T. Placke, New insights into the uptake/release of FTFSI- anions into graphite by means of in situ powder X-ray diffraction, *Electrochem. Commun.* 71 (2016) 52-55.
- [136] S. Aladinli, F. Bordet, K. Ahlbrecht, J. Tuebke, M. Holzapfel, Compositional graphitic cathode

investigation and structural characterization tests for Na-based dual-ion battery applications using ethylene carbonate:ethyl methyl carbonate-based electrolyte, *Electrochim. Acta* 228 (2017) 503-512.

[137] M. Balabajew, H. Reinhardt, N. Bock, M. Duchardt, S. Kachel, N. Hampp, B. Roling, In-situ raman study of the intercalation of bis(trifluoromethylsulfonyl) imid Ions into graphite inside a dual-ion cell, *Electrochim. Acta* 211 (2016) 679-688.

[138] H. He, H. Wang, D. Sun, M. Shao, X. Huang, Y. Tang, N-doped rutile TiO<sub>2</sub>/C with significantly enhanced Na storage capacity for Na-ion batteries, *Electrochim. Acta* 236 (2017) 43-52.

[139] P. Meister, O. Fromm, S. Rothermel, J. Kasnatscheew, M. Winter, T. Placke, Sodium-based vs. lithium-based dual-ion cells: electrochemical study of anion intercalation/de-intercalation into/from graphite and metal plating/dissolution behavior, *Electrochim. Acta* 228 (2017) 18-27.

[140] L. Yan, H. Yu, S. Qian, P. Li, X. Lin, N. Long, R. Zhang, M. Shui, J. Shu, Enhanced lithium storage performance of Li<sub>5</sub>Cr<sub>9</sub>Ti<sub>4</sub>O<sub>24</sub> anode by nitrogen and sulfur dual-doped carbon coating, *Electrochim. Acta* 213 (2016) 217-224.

[141] C. Liu, X. Ma, F. Xu, L. Zheng, H. Zhang, W. Feng, X. Huang, M. Armand, J. Nie, H. Chen, Z. Zhou, Ionic liquid electrolyte of lithium bis(fluorosulfonyl)imide/N-methyl-N-propylpiperidinium bis(fluorosulfonyl)imide for Li/natural graphite cells: Effect of concentration of lithium salt on the physicochemical and electrochemical properties, *Electrochim. Acta* 149 (2014) 370-385.

[142] S. Tsujioka, B.G. Nolan, H. Takase, B.P. Fauber, S.H. Strauss, Conductivities and electrochemical stabilities of lithium salts of polyfluoroalkoxyaluminate superweak anions, *J. Electrochem. Soc.* 151(9) (2004) A1418-A1423.

[143] S. Wang, S. Jiao, J. Wang, H.S. Chen, D. Tian, H. Lei, D.N. Fang, High-performance aluminum-ion battery with CuS@C microsphere composite cathode, *ACS Nano* 11(1) (2017)

469-477.

[144] S. Lee, J. Cho, Critical requirements for rapid charging of rechargeable Al- and Li-ion batteries, *Angew. Chem. Int. Ed.* 54(33) (2015) 9452-9455.

[145] L. Fu, N. Li, Y. Liu, W. Wang, Y. Zhu, Y. Wu, Advances of aluminum based energy storage systems, *Chin. J. Chem.* 35(1) (2017) 13-20.

[146] G.A. Elia, I. Hasa, G. Greco, T. Diemant, K. Marquardt, K. Hoepfner, R.J. Behm, A. Hoell, S. Passerini, R. Hahn, Insights into the reversibility of aluminum graphite batteries, *J. Mater. Chem. A* 5(20) (2017) 9682-9690.

[147] D. Kubo, K. Tadanaga, A. Hayashi, M. Tatsumisago, Multifunctional inorganic electrode materials for high-performance rechargeable metal-air batteries, *J. Mater. Chem. A* 1(23) (2013) 6804-6809.

[148] J. Zhao, Y. Tian, Z. Wang, S. Cong, D. Zhou, Q. Zhang, M. Yang, W. Zhang, F. Geng, Z. Zhao, Trace H<sub>2</sub> O<sub>2</sub> -assisted high-capacity tungsten oxide electrochromic batteries with ultrafast charging in seconds, *Angew. Chem. Int. Ed.* 55(25) (2016) 7161-7165.

[149] Z. Chen, W. Ren, L. Gao, B. Liu, S. Pei, H.M. Cheng, Three-dimensional flexible and conductive interconnected graphene networks grown by chemical vapour deposition, *Nat. Mater.* 10(6) (2011) 424-428.

[150] X.G. Sun, Z. Bi, H. Liu, Y. Fang, C.A. Bridges, M.P. Paranthaman, S. Dai, G.M. Brown, A high performance hybrid battery based on aluminum anode and LiFePO<sub>4</sub> cathode, *Chem. Commun.* 52(8) (2016) 1713-1716.

[151] Y. Wu, M. Gong, M.C. Lin, C. Yuan, M. Angell, L. Huang, D.Y. Wang, X. Zhang, J. Yang, B.J. Hwang, H. Dai, 3D graphitic foams derived from chloroaluminate anion intercalation for



ultrafast aluminum-ion battery, *Adv. Mater.* 28(41) (2016) 9218-9222.

[152] H. Chen, F. Guo, Y. Liu, T. Huang, B. Zheng, N. Ananth, Z. Xu, W. Gao, C. Gao, A defect-free principle for advanced graphene cathode of aluminum-ion battery, *Adv. Mater.* 29(12) (2017) 1605958.

[153] H. Chen, H. Xu, S. Wang, T. Huang, J. Xi, S. Cai, F. Guo, Z. Xu, W. Gao, C. Gao, Ultrafast all-climate aluminum-graphene battery with quarter-million cycle life, *Sci. Adv.* 3(12) (2017) eaao7233.

[154] L. Zhang, L. Chen, H. Luo, X. Zhou, Z. Liu, Large-sized few-layer graphene enables an ultrafast and long-life aluminum-ion battery, *Adv. Energy Mater.* 7(15) (2017) 1700034.

[155] N. Gunawardhana, G.-J. Park, A.K. Thapa, N. Dimov, M. Sasidharan, H. Nakamura, M. Yoshio, Performance of a graphite (KS-6)/MoO<sub>3</sub> energy storing system, *J. Power Sources* 203 (2012) 257-261.

[156] X. Shi, T. Deng, B. Zhang, W. Zhang, L. Sui, H. Yang, D. Wang, W. Shi, C.M. Chen, W. Zheng, Accessible 3D integrative paper electrode shapes: all - carbon dual - ion batteries with optimum packaging performances, *ChemElectroChem* 4(12) (2017) 3238-3243.

[157] J.A. Read, In-situ studies on the electrochemical intercalation of hexafluorophosphate anion in graphite with selective cointercalation of solvent, *J. Phys. Chem. C* 119(16) (2015) 8438-8446.

[158] X. Zhang, Y. Tang, F. Zhang, C.-S. Lee, A novel aluminum-graphite dual-ion battery, *Adv. Energy Mater.* 6(11) (2016) 1502588.

[159] F. Zhang, B. Ji, X. Tong, M. Sheng, X. Zhang, C.-S. Lee, Y. Tang, A dual-ion battery constructed with aluminum foil anode and mesocarbon microbead cathode via an alloying/intercalation process in an ionic liquid electrolyte, *Adv. Mater. Interfaces* 3(23) (2016)

1600605.

[160] X. Tong, F. Zhang, B. Ji, M. Sheng, Y. Tang, Carbon-coated porous aluminum foil anode for high-rate, long-term cycling stability, and high energy density dual-ion batteries, *Adv. Mater.* 28(45) (2016) 9979-9985.

[161] P. Qin, M. Wang, N. Li, H. Zhu, X. Ding, Y. Tang, Bubble-sheet-like interface design with an ultrastable solid electrolyte layer for high-performance dual-ion batteries, *Adv. Mater.* 29(17) (2017) 1606805.

[162] C. Jiang, Y. Fang, J. Lang, Y. Tang, Integrated configuration design for ultrafast rechargeable dual-ion battery, *Adv. Energy Mater.* 7(19) (2017) 1700913.

[163] J. Peng, N. Chen, R. He, Z. Wang, S. Dai, X. Jin, Electrochemically driven transformation of amorphous carbons to crystalline graphite nanoflakes: a facile and mild graphitization method, *Angew. Chem. Int. Ed.* 129(7) (2017) 1777-1781.

[164] M. Sheng, F. Zhang, B. Ji, X. Tong, Y. Tang, A novel tin-graphite dual-ion battery based on sodium-ion electrolyte with high energy density, *Adv. Energy Mater.* (2016) 1601963.

[165] B. Ji, F. Zhang, N. Wu, Y. Tang, A dual-carbon battery based on potassium-ion electrolyte, *Adv. Energy Mater.* 7(20) (2017) 1700920.

[166] B. Ji, F. Zhang, X. Song, Y. Tang, A novel potassium-ion-based dual-ion battery, *Adv. Mater.* 29(19) (2017) 1700519.

[167] E. Zhang, W. Cao, B. Wang, X. Yu, L. Wang, Z. Xu, B. Lu, A novel aluminum dual-ion battery, *Energy Storage Mater.* 11(Supplement C) (2018) 91-99.

[168] M. Lee, J. Hong, B. Lee, K. Ku, S. Lee, C.B. Park, K. Kang, Multi-electron redox phenazine for ready-to-charge organic batteries, *Green Chem.* 19(13) (2017) 2980-2985.

- [169] M. Kazazi, Synthesis and elevated temperature performance of a polypyrrole-sulfur-multi-walled carbon nanotube composite cathode for lithium sulfur batteries, *Ionics* 22(7) (2016) 1103-1112.
- [170] Y. Wu, L. Zhan, K. Huang, H. Wang, H. Yu, S. Wang, F. Peng, C. Lai, Iron based dual-metal oxides on graphene for lithium-ion batteries anode: Effects of composition and morphology, *J. Alloys Compd.* 684 (2016) 47-54.
- [171] Y. Cheng, H.J. Chang, H. Dong, D. Choi, V.L. Sprenkle, J. Liu, Y. Yao, G. Li, Rechargeable Mg-Li hybrid batteries: status and challenges, *J. Mater. Res.* 31(20) (2016) 3125-3141.
- [172] W. Liu, X. Li, M. Zhu, X. He, High-performance all-solid state asymmetric supercapacitor based on Co<sub>3</sub>O<sub>4</sub> nanowires and carbon aerogel, *J. Power Sources* 282 (2015) 179-186.
- [173] T.A. Zegeye, C.-F.J. Kuo, A.S. Wotango, C.-J. Pan, H.-M. Chen, A.M. Haregewoin, J.-H. Cheng, W.-N. Su, B.-J. Hwang, Hybrid nanostructured microporous carbon-mesoporous carbon doped titanium dioxide/sulfur composite positive electrode materials for rechargeable lithium-sulfur batteries, *J. Power Sources* 324 (2016) 239-252.
- [174] S.-D. Seo, C. Choi, D.-W. Kim, Fabrication of sulfur-impregnated porous carbon nanostructured electrodes via dual-mode activation for lithium-sulfur batteries, *Mater. Lett.* 172 (2016) 116-119.
- [175] S. Dong, Z. Li, I.A. Rodriguez-Perez, H. Jiang, J. Lu, X. Zhang, X. Ji, A novel coronene//Na<sub>2</sub>Ti<sub>3</sub>O<sub>7</sub> dual-ion battery, *Nano Energy* 40 (2017) 233-239.
- [176] X. Han, X. Wu, C. Zhong, Y. Deng, N. Zhao, W. Hu, NiCo<sub>2</sub>S<sub>4</sub> nanocrystals anchored on nitrogen-doped carbon nanotubes as a highly efficient bifunctional electrocatalyst for rechargeable zinc-air batteries, *Nano Energy* 31 (2017) 541-550.

- [177] Y. Li, Q. An, Y. Cheng, Y. Liang, Y. Ren, C.-J. Sun, H. Dong, Z. Tang, G. Li, Y. Yao, A high-voltage rechargeable magnesium-sodium hybrid battery, *Nano Energy* 34 (2017) 188-194.
- [178] S. Wang, S. Jiao, D. Tian, H.-S. Chen, H. Jiao, J. Tu, Y. Liu, D.-N. Fang, A novel ultrafast rechargeable multi-ions battery, *Adv. Mater.* 29(16) (2017) 1606349.
- [179] N. Gunawardhana, G.J. Park, N. Dimov, A.K. Thapa, H. Nakamura, H.Y. Wang, T. Ishihara, M. Yoshio, Constructing a novel and safer energy storing system using a graphite cathode and a MoO<sub>3</sub> anode, *J. Power Sources* 196(18) (2011) 7886-7890.
- [180] L. Fan, Q. Liu, Z. Xu, B. Lu, An organic cathode for potassium dual-ion full battery, *ACS Energy Lett.* 2(7) (2017) 1614-1620.
- [181] I.A. Rodriguez-Perez, Z. Jian, P.K. Waldenmaier, J.W. Palmisano, R.S. Chandrabose, X. Wang, M.M. Lerner, R.G. Carter, X. Ji, A hydrocarbon cathode for dual-ion batteries, *ACS Energy Lett.* 1(4) (2016) 719-723.
- [182] P. Srimuk, J. Halim, J. Lee, Q. Tao, J. Rosen, V. Presser, Two-dimensional molybdenum carbide (MXene) with divacancy ordering for brackish and seawater desalination via cation and anion intercalation, *ACS Sustainable Chem. Eng.* 6(3) (2018) 3739-3747.
- [183] T.B. Schon, B.T. McAllister, P.F. Li, D.S. Seferos, The rise of organic electrode materials for energy storage, *Chem. Soc. Rev.* 45(22) (2016) 6345-6404.